Supercooled nano-droplets of water confined in hydrophobic rubber

R. Neffati, P. Judeinstein, J. Rault

Supercooled nano-droplets of water confined in hydrophobic rubber

R. Neffati [1,4*], P. Judeinstein [2,3], J. Rault [2]

(1) Department of Physics, King Khalid University P. Box 9032, Abha 61413 - Kingdom of Saudi Arabia

(2) *Université Paris-Saclay, CNRS, Laboratoire de Physique des Solides, 91405, Orsay, France*

(3) *Université Paris-Saclay, CNRS, CEA, Laboratoire Léon Brillouin, 91191, Gif-sur-Yvette, France*

(4) *IPEIN, University of Carthage, Campus of El Mrazga, P. Box 62, Nabeul 8000, Tunisia*

(*) Corresponding Author: riadhneffti@gmail.com, or ryad@kku.edu.sa

GRAPHICAL ABSTRACT.

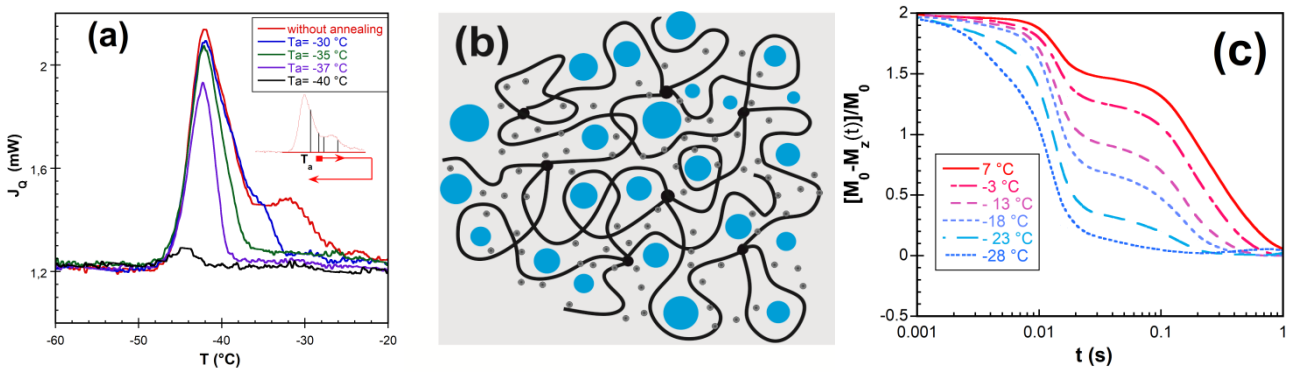

(a) Partial crystallization of nano droplets of water by successive annealing at different temperatures

(b) Blue spheres represent water droplet inside, a hydrophobic elastomers and the other dark spots are possible hydrophilic sites which are side product of vulcanization. The size distribution of these nano droplets is bimodal as reveal by their freezing and ^{2}H-NMR relaxometry.

(c) The decrease with time of the relative deuterium magnetization of heavy water after an inverse recovery sequence is not a single exponential and one could deduce by inverse Laplace transformation the distributions of spin-lattice relaxation time.

Abstract.

Hydrophobic elastomers are capable of absorbing water which forms droplets around hydrophilic sites. The freezing-melting as well as the dynamics of water nano-droplets in butyl rubber are affected as revealed by differential scanning calorimetry (DSC) and deuterium nuclear magnetic resonance (^{2}H-NMR). Upon cooling down all water crystalizes as bimodal droplets population (d_a=3.4 nm and d_b=4.4 nm) in a temperature range associated to droplet's size distribution. Contrary, melting temperature is not shifted according to Gibbs-Thomson relation; this is explained by an addition effect due to embedding water droplets in hydrophobic surrounding. The dynamics of supercooled water is studied at different temperature and hydration ratio using the ^{2}H-NMR spin-lattice relaxation rate. The relative decrease of the longitudinal magnetization is not a single exponential and one deduced by numerical inverse Laplace transformation the distribution of spin-lattice relaxation time which turnout to be bimodal in agreement with DSC measurements ($T_{1,a}$ ~10 ms and $T_{1,b}$ ~200 ms). As deduced from the spin-lattice relaxation, correlation time of molecular reorientation in water droplet is longer than bulk water (there is a slowdown of molecular reorientation) and the behavior with temperature follows VFT equations with a changing fragility as droplet size is reduced when reducing hydration.

Key words: water droplet, hydrophobic elastomers, crystallization, melting, ^{2}H-NMR relaxometry, VFT equation.

INTRODUCTION

Understanding hydrophobicity at the molecular level continue to be the focus of many research [1-5] due to its importance in biological systems [1, 6], in surfactant sciences and industry [7] but also in hydrophobic elastomers [8, 9] which are the focus of this paper. In his seminal work, Kauzmann [10], pointed out the association of water molecules induced by apolar groups in aqueous environment. Since then tremendous theoretical and simulation efforts was done to understand processes accompanying hydrophobic hydration [11-19] particularly the molecular origin of the "iceberg" model. Recently, many experimental research focused on the behaviour of water confined in hydrophobic environment [20-24]. Simulations of water confined by hydrophobic surfaces [25-31] were used to investigate the dynamic and thermodynamic behaviour of water molecules in extreme hydrophobic confinement conditions. In almost all the former experimental and simulation investigations, confinement of water is found to disrupt the hydrogen bonding network (HNB) and consequently affects water's dynamics, structural and thermodynamic features. In addition, the interaction of water-surface or water-surrounding is of primary importance in determining the mobility and thermodynamics behaviour of confined water. Most of the experimental investigations in porous glasses needs its modification so that the pore's surface becomes more or less hydrophobic and often one faces the practical problem of introducing water inside these host material while hydrophobic elastomer does not need such modification and has the ability to absorb water vapour at relatively high temperature. In fact, hydrophobic rubber coatings are often used to avoid water penetration and prohibit problems associated to its presence like corrosion or any other material performance deterioration. Therefore, absorption of water by hydrophobic elastomers, was subject of research by polymer scientists [8, 32]. It is proven that water in hydrophobic elastomers is dispersed as

droplets [8, 9, 32, 33]. The water droplets are believed to form around hydrophilic sites which are side product of the rubber vulcanizations [34] or small relatively hydrophilic chemical groups. Butyl rubber (BR) has a highly saturated backbone, and presents hence high impermiability to water vapour and gas, making it a good candidate for insulating and protective coatings in addition to his damping performance. For scientist focusing on water behaviour in confined hydrophobic environment, butyl rubber is hence an excellent host material.

In order to understand freezing-melting under confinement, it is worth mentioning that crystallization is governed by both nucleation and growth processes in bulk liquids [35]. Nevertheless, when liquids are introduced in a host material, one of the former two processes could dominate the crystallization behaviour depending on the dispersion of the liquid. In fact, in the case of hydrogels for example the Tg-regulation model was introduced when crystal growth is arrested by the glass transition of the system [36], whereas when separated droplets are confined in host material, it is nucleation which becomes a driving process [37, 38]. In contrast to crystallization, melting is a first order thermodynamic transitions occurring while having equilibrium between the solid and liquid phases. The dynamic of water under sever confinement has received intensive attention last decades, particularly the fragile-strong transitions predicted at about 225K is subject of intensive debate [39-43].

NMR is a powerful experimental tool for following the behavior of confined liquids in porous materials [44-49] or in polymer [50, 51]. In confined liquids, and under the fast-exchange condition [45, 52], one measures average relaxation rates $R_i = 1/T_i$ for transverse (i=2 : spin-spin) , or longitudinal (i=1 : spin-lattice) nuclear magnetization which have two limiting regimes diffusion-limited (DL) or surface-limited (SL) depending on whether respectively $4D \ll xd/T_s$ or $4D \gg xd/T_s$ where D is the self-diffusion coefficient, d is the confinement diameter, x the thickness of the liquid at the interface having a

typical relaxation time T_s. For example in porous glass govern the nuclear magnetic relaxation [49].

In this paper one will first study the freezing –melting transitions of water droplets confined inside the hydrophobic rubbery matrix (BR) using DSC and the intensity of ^{2}H-NMR signal of deuterated water. These results are correlated to the droplets size distribution. The dynamics of water at different hydration and temperature will be followed through the spin-lattice relaxation time measurement of ^{2}H-NMR. One will also point out how this droplet size distribution induces a distribution also in water dynamics since this later is also size depend as will be discussed.

EXPERIMENTAL

A reaction mixture composed of 100 g POLYSAR butyl rubber 400, 5 g of ZnO, 3g of benzothiazyl-sulfonmorphilid (VULKOCIT MOZ) ,1.5 g of methyl-mercapto-benzimidazole (VULKANOX MB 2), and 2 g of sulfur was held in a Teflon mold at 150°C during 30 min under pressure. The sulfur vulcanization process, activated by mean of zinc oxide (ZnO) is a well-established process in rubber industry [53, 54]. From other side, the dispersed ZnO could constitute hydrophilic sites where water droplets can eventually form when water vapor is forced to inter the hydrophobic elastomer. In our case, water was forced during about 21 days to enter the hydrophobic matrix at temperature about 80°C as was the case in previous work about the same kind of material [33]. Then samples of about 1.5 cm x 1.5 cm x 0.1 cm were kept in pure water at room temperature. The water content is expressed in term of hydration rate $h = m_w / m_0$ where m_w is the mass of water and m_0 is the mass of the dry rubber. All masses were measured using a high precision Mettler Balance (± 0.1mg). Small DSC samples with total mass around 5 mg were cut from these original sample. In order, to perform ^{2}H-NMR dried sample was kept at 80°C for a three weeks in deuterated water to allow the deuterated water droplet formation. The

drying was performed by keeping samples at the same temperature 80°C with hygroscopic silica gel in a desiccator and regular monitoring of mass and DSC signal. DSC thermograms are recorded using a DSC30 Mettler with TA3000 processing unit. After standard calibration, different scanning rates were performed first on distilled and degasified water then on the samples. The cooling/heating rates ± 5 °C/min were used to have acceptable signal/noise ratio. Lower scanning rates (± 1 °C/min) were used in order to apply thermoporosimetry as introduced by Brun [55] to link the crystallization thermogram to the droplet size distribution or to analyse melting behaviour at equilibrium [9, 49].

A Bruker spectrometer with static field $B_0 = 5.87\ T$ corresponding to a deuterium Larmor's frequency about ω_0 = 38.376 MHz was used for NMR measurements. The spectrometer was equipped with 5 mm broad band probe used without frequency lock control and temperature control unit with ± 0.5 °C stability. Standard temperature calibration methods using ethylene glycol reference tube in low temperature measurement where liquid nitrogen was used as cold source. The pulse width for rotating the nuclear magnetization by an angle 90° was first evaluated to 16.5 μs. The inverse recovery sequence (180°-τ-90°), was applied for measuring the spin-lattice T_1 relaxation times [56]. Since we're using a liquid NMR spectrometer with a moderate acquisition spectral window (± 20 kHz), the solid signal vanishes as in cryoporometry experiments [48, 57] where only the signal from liquid parts inside the system is acquired.

RESULTS AND DISCUSSION

Figure 1 presents DSC thermograms of water crystallization (figure 1a) and melting of the formed ice (figure 1b) inside butyl rubber at different hydration. All the crystallization thermograms were obtained by cooling from 10 °C down to -90°C at a scanning rate -5°C/mn (figure 1a) then immediately heating

up to acquire the melting thermograms at the scanning rate +5 °C/mn (figure1b). Obviously, crystallization thermograms are shifted as one could expect due to confinement. However, melting thermograms are surprisingly much less shifted. Despite their different swelling ratio, all samples have an unchanged glass transition temperature around T_g = -67.5 °C as shown in the inset of figure 1b. The absence of the plasticizing effect confirms that water is not dispersed at the molecular level in the rubbery matrix as it was expected. In fact, it is well known that when a solvent with lower glass transition temperature is mixed at the molecular level to a polymeric host material the glass transition of the whole mixture is lowered [36]. Here since we have no such effect we could deduce that water is not dispersed at the molecular level and hence it is accumulated in the form of droplets in line with swelling of rubbers by water [8, 32] or other studies on the same kind of materials [9, 33]. The crystallization thermograms are composed of two peaks, associated with bimodal size distribution of droplets as will be discussed in following sections. The biggest peak around -45°C has the highest surface (about 80 % of the total crystallization surface) whereas the smaller crystallization peak (about 20 % the total surface) is around -35 °C. The two crystallization peaks are shifted to lower temperature due to the scanning rate as well as the high thermal resistance of rubber these technical corrections are discussed elsewhere [9]. The inset in figure 1a depicts the effect of scanning rate on DSC crystallization thermograms of the sample with the highest hydration (34.5%). The scanning rate 1°C/min was found to be the closest to the "true" thermogram obtained by successive annealing [9]. In addition, operating different annealing in the crystallization or melting intervals proved also that there is no any connection between these dispersed water droplets. At low scanning rate, the temperature of the two crystallization peak extrapolates respectively to -38°C and -29.5°C. The two crystallization peaks could be associated with droplets sizes respectively 1.7 nm and 2.2 nm if one uses Brun's relation $\Delta T_c \simeq 64.6\ nm / r$ [55], where $\Delta T_c = T_m^0 - T_c$ is the supercooling taking as reference the melting point of the bulk pure liquid. It is worth mentioning that

Petrov et al. [48] gave independently almost the same equation $r(nm) \simeq 3\,\mathrm{k}_c / \Delta T_c$ with $k_c = 25\ nm\ K$ for spherical pores in NMR cryoporometry. According to Gibbs-Thomson [49, 58] relation widely verified in porous media for melting [t_m~0.18/d(nm)] which is also the same used in NMR cryoporometry for melting $r(nm) \simeq 2\,\mathrm{k}_c / \Delta T_m$, The melting transition should be shifted about 24.6 °C if one accepted size about 2nm. Obviously this is not the case, in fact at low scanning rate thermograms starting extrapolates to about -6.5 °C which clearly gives a crystal radius of about 7.5 nm. The 18 °C difference in shift corresponds to $t_m = (T_m^0 - T_m) / T_m^0 = 0.066 \simeq -\Delta\mu / \Delta H_m^0$ meaning that one has an effect associated to change of the chemical potential of 6.6% the melting enthalpy counterbalancing the finite size effect. Such effect is what insure the equilibrium swelling ratio of hydrophobic elastomer [8]. In fact, according to Thomas and Muniandy [8] the elastomeric matrix exert a pressure *p* opposing the growth of the droplet size and at equilibrium one has equality of the osmotic pressure inside the droplet and this pressure when the rubber is in pure liquid bath. The other possible contribution to chemical potential is given by the energetic cost of hydrophobic hydration which according to chandler [4] for a hydrophobic droplet of radius r in water is given by $4\pi\gamma_{\mathrm{lg}} \cdot r^2 + \frac{4\pi}{3} r^3 \cdot p$ .Finally it is worth mentioning that the melting shift is usually linked to the change of the chemical potential compared to pure liquid $\Delta\mu$ resulting from any external process. Since the swelling equilibrium of polymeric networks is always associated with $\Delta\mu_{eq} = 0$, one usually has less shift of the melting point of solvent crystals compared to the solutions case or the pure confinement in porous materials. From the crystallization curves, one could notice that as the rubber becomes more hydrated, the relative intensity of the two mentioned peaks changes but without much shift of the peak's position. Figure 2a depicts the integrated enthalpies of crystallization and melting for different hydration of butyl rubber. The surface of the sample prepared for DSC does not contain any free water that is why there is no peak associated to bulk water.

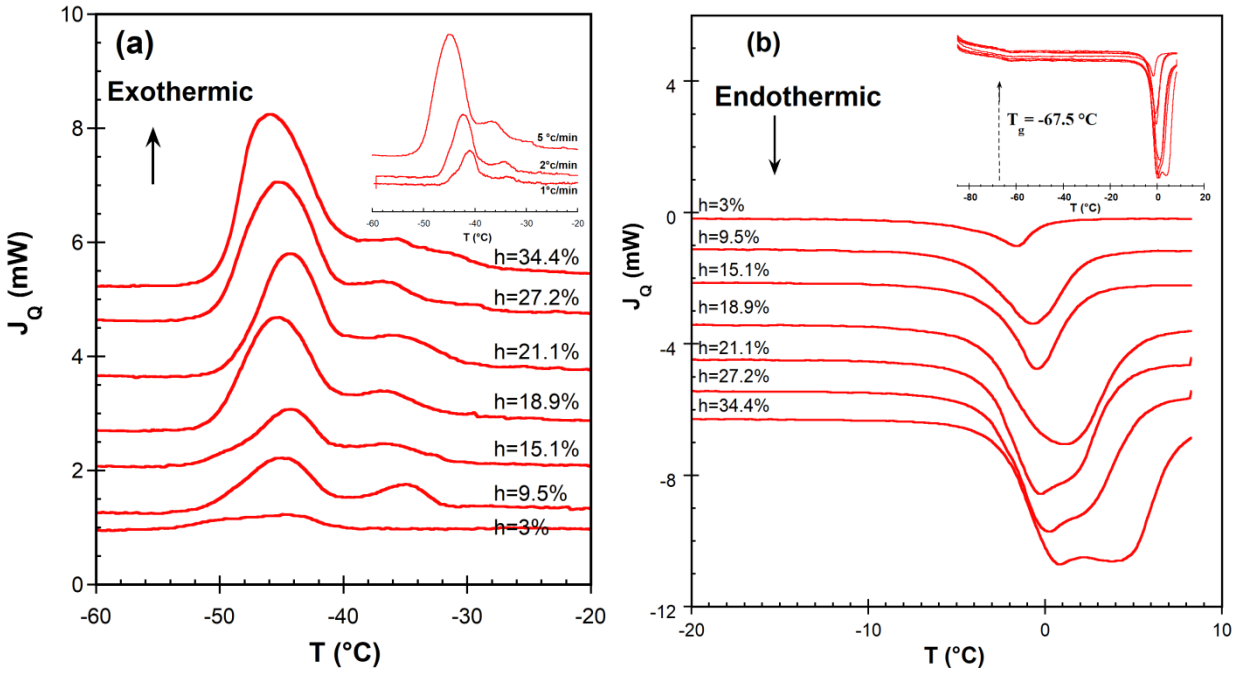

FIGURE 1. **(a)** Crystallization thermograms at -5 °C/min for different hydration rates of butyl rubber, the inset is thermograms at different scanning rates for the sample with h =34.4%. **(b)** Melting part of thermograms at 5 °C/min the inset shows the whole melting thermograms with the rubber glass transition.

The total melting or crystallization enthalpies increase nonlinearly with the hydration rate which is a typical feature of confined water [49]. One reports also on the same figure 2a, the integration of the two peaks forming the crystallization thermograms associated two droplets sizes d_1 and d_2. Figure 2b depicts the proportion variation of the two droplets populations with hydrations. These proportions are calculated from the surface of the corresponding DSC peak over the total surface. The proportions of the two droplets populations remains almost constant around 80% and 20% respectively for the droplets with size about r_2=(1.7±0.2) nm and r_1=(2.2±0.2) nm.

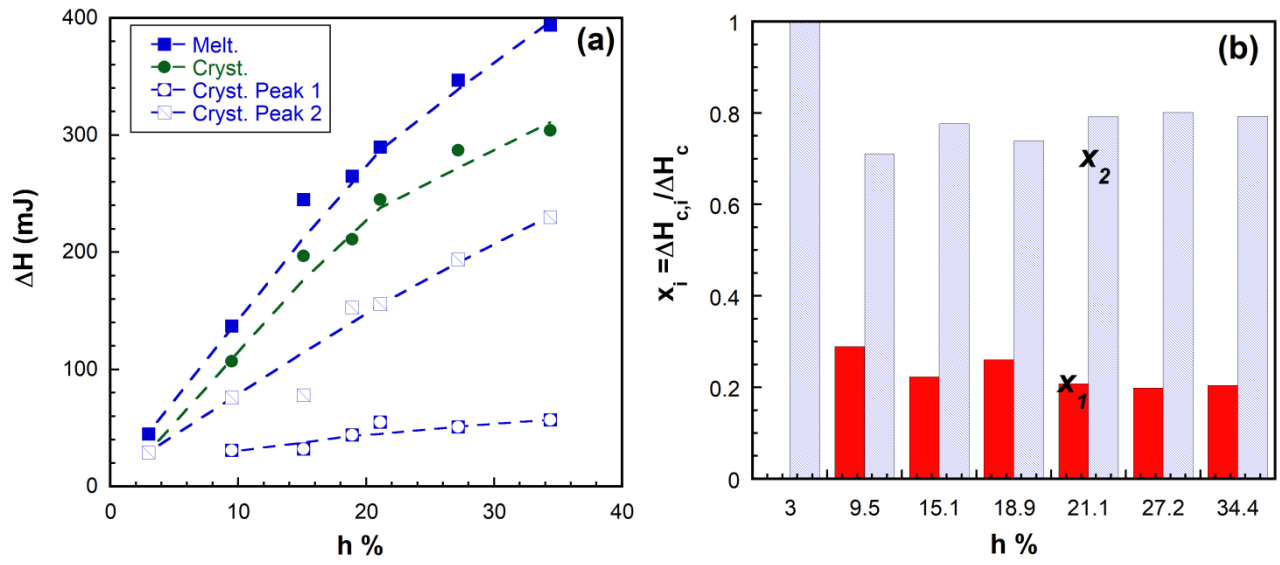

FIGURE 2. **(a)** Enthalpies of crystallization and melting at different hydrations of butyl rubber as well as the integration of the two crystallization peaks at -45°C and -35°C when using -5°C/min as scanning rate. **(b)** the relative proportions of the two peaks (associated to the two droplets sizes) for different hydrations.

Figure 3a shows crystallization thermograms, obtained after annealing during 20 min at temperature T_a= -30°C, -35°C, -37°C and -40°C, situated in the crystallization interval. This figure could be an experimental proof of droplet disconnection and that each given temperature is associated to a droplet size. In fact, if water form a connected zone or network (as in porous media), any annealing in the crystallization zone could lead to a propagation of the freezing the whole network. Since droplets are disconnected, the crystallization process is governed by nucleation. This process is indeed proven to be size dependent [38] and hence crystallization occurs progressively from the biggest droplet sizes to the lowest ones as temperature drops down. Supposing that crystallization in a given droplet occurs at the temperature T when the critical nuclei radius *r* as estimated from the classic nucleation theory reaches the droplet radius one could write then [59]:

$$\ln\left(\frac{T}{T_m^0}\right) = -\frac{2\gamma_{ls}v_l}{r\Delta H_m^0} \qquad (1)$$

which allows to establish a relation between the size and the temperature scale. T_m^0 and ΔH_m^0 are respectively the melting temperature and enthalpy of bulk water and γ_{ls} is the ice-water surface tension. Noticing that $t_c = \left(T_m^0 - T_c\right)/T_m^0 \ll 1$, one could obtain by expansion ($\ln\left(\frac{T_c}{T_m^0}\right) = \ln(1-t_c) \sim -t_c$) the same kind of Gibbs-Thomson relation for crystallization $\Delta T_c = A_c / r$ where $A_c = 2\gamma_{ls} v_l T_m^0 / \Delta H_m^0$, but with different coefficient as noted by different authors [48, 55]. For water we took the average value available in former references A_c~70 nm K when the radius is in nm [48, 55]. It is worth mentioning here that in order to convert a DSC thermogram into size distribution the scanning rate should be very low to avoid technical broadening [9]. Figure 3b gives the normalized droplet size distribution deduced from a thermograms at 1°C/min as scanning rate for samples with hydration rate h=21.1%. On could notice that the size distribution is bimodal centered around typical droplet radius r_a~1.7 nm and r_b~2.2 nm, in agreement with previous DSC and X rays measurements [9, 33].

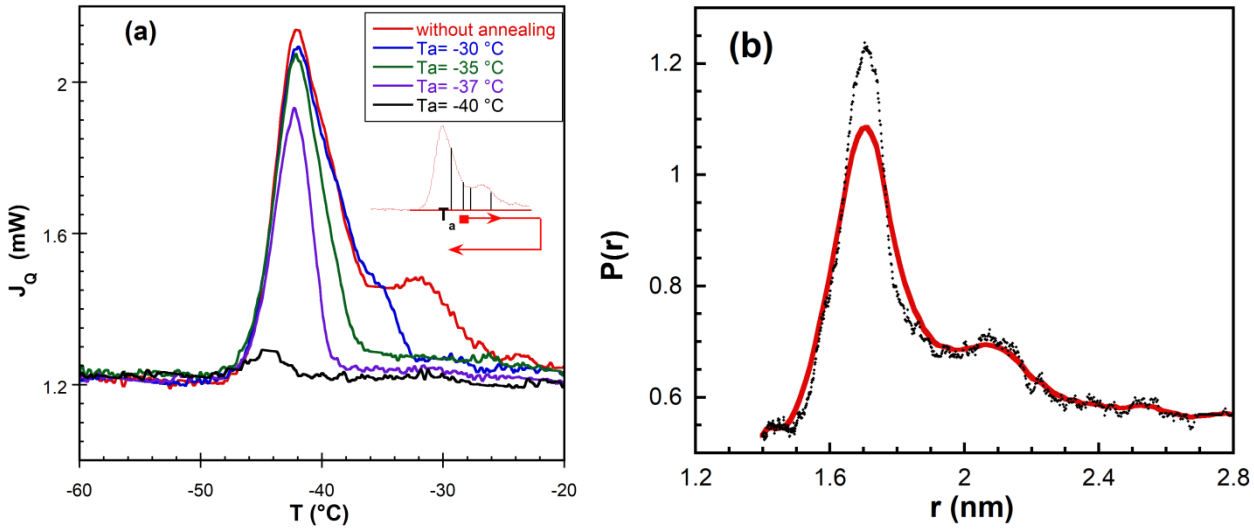

FIGURE 3. (a) Crystallization thermograms after annealing at T_a during 20 min then heating at + 5 °C/min up to -8 °C and finally cooling at -5°C/ **(b)** Size distribution deduced from crystallization thermogram at 1°C/min of the sample with h= 21.1%.

Figure 4a depicts the variation of the ^{2}H-NMR intensity during the cooling stage fo the "swollen" butyl rubber samples. One could notice that below 235 K the signal intensity is zero which is an experimental confirmation that all water crystalizes in contrast with hydrophilic porous media [49] or hydrophilic polymers [36] where a fraction of water does not crystalize. Since water is in form of droplets around hydrophilic sites, one could use NMR cryoporometry to give another estimation of the droplet sizes. Figure 4b gives such estimation of droplets sizes where one converted the temperature scale using $\Delta T_c = 3k_c / r$ as done in typical cryoporometry studies where we could use the value for water with k_c =25 nm K corresponding typically to ice-water surface tension about γ_{sl} = 30 mJ/m^2 [48]. It is worth mentioning that during each temperature the waiting time for temperature equilibration, the acquisition of the FID and the T_1 measure via the inverse recovery procedure insures that indeed one is at equilibrium and no effect of scanning rate as in DSC measurements.

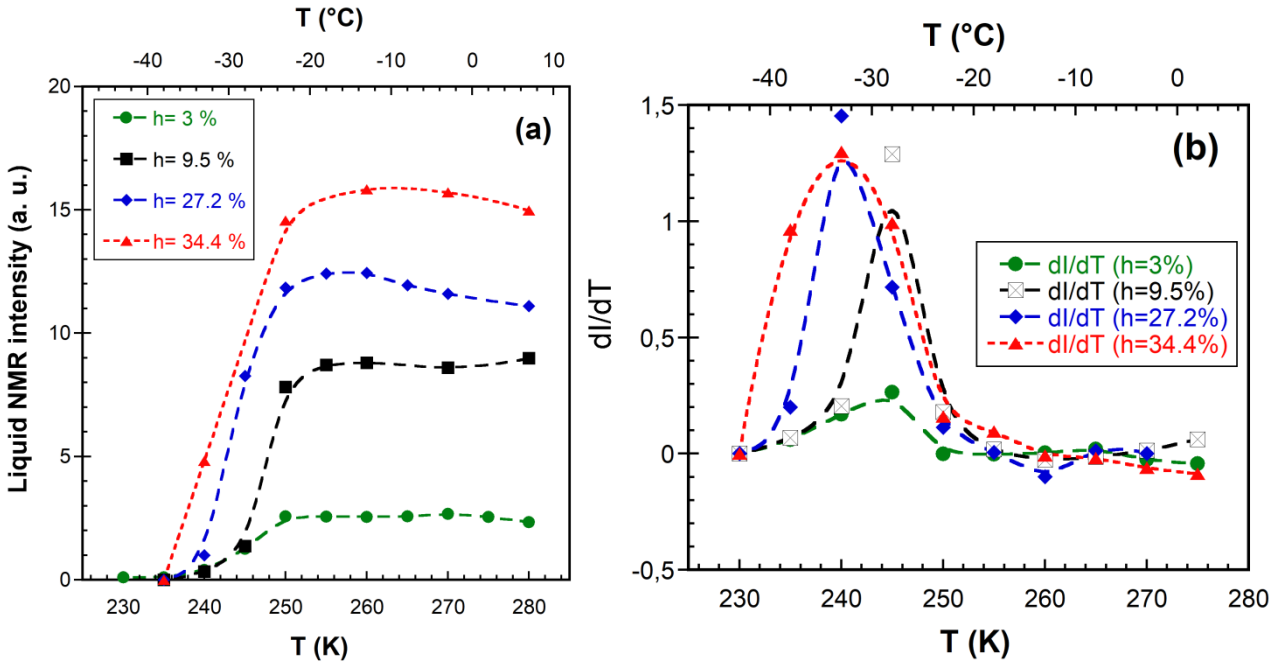

FIGURE 4. (**a**) ^{2}H-NMR intensity versus T for sample with different hydration. (**b**) Derivative of the NMR ^{2}H intensity versus temperature which gives the size distributions of droplets (cryoporometry).

Figure 5a gives the decrease of the relative longitudinal nuclear magnetization $(M_0 - M_z(t))/M_0$ with time, where M_0 is the equilibrium magnetization before the application of the inverse recovery sequence. This decrease is plotted for different hydrations at the same temperature T=285 K where clearly we could notice that the relaxation is not a single exponential. Therefore, one should consider a distribution of spin-lattice relaxation rates which is related to the variation of the longitudinal nuclear magnetization after an inverse recovery sequence by:

$$M_z(t) = M_0 \cdot \left[1 - 2 \cdot \int P(R_1) \cdot e^{-R_1 t} \cdot dR_1\right] \qquad (2)$$

One could obtain the distribution of the longitudinal relaxation times, by operating an inverse Laplace transformation of the quantity $(M_0 - M_z)/M_0$, as depicted in figure 5b. The numerical Laplace transformation of the relative decrease of the longitudinal nuclear magnetization $(M_0 - M_z)/M_0$ was done using CONTIN algorithm [60] through a plugin within Originlab software followed by numerical normalization. This distribution of the longitudinal magnetization relaxation time is correlated to the size distribution of droplets through equation (4). In fact, for spherical water droplet with typical diameter d and having a shell with thickness x at the interface assumed to has a different relaxation rate $1/T_{1s}$, one can neglect the bulk relaxation rate and write the mean resulting spin-lattice relaxation time due to fast exchange as [45]:

$$\frac{T_{1s}}{T_1(d)} \simeq \cdot \frac{6x/d}{1 + xd/(4T_{1s}D)} \qquad (3)$$

Obviously if one consider x~1nm, d=4nm, T_{1s} 1ms and a typical diffusion coefficient about 10^{-5} cm^2/s [61] then $xd/T_{1s} \ll D$ and consequently the relaxation is surface limited process, in such case :

$$\frac{1}{T_1(d)} \simeq \frac{6x/d}{T_{1s}} \qquad (4)$$

Obviously the distribution of the spin-lattice relaxation time is also bimodal with two distinguished relaxations times $T_{1,a}$ ~10 ms and $T_{1,b}$ ~200 ms as depicted in figure 5b. On the same figure one could notice that we have the same proportion found in DSC with respectively the two droplet sizes r_a~1.7 nm and r_b~2.2 nm. This concordance is argued by the fact that from equation (4), we could clearly deduce that the smaller the droplet size is the higher is the relaxation rate. However, assuming that relaxation rate of water at droplet's surface surrounded by the hydrophobic rubber is the same for the two droplets populations, one cannot explain the difference between the mean relaxation times only by the difference in the droplet sizes because $d_b / d_a \simeq 1.3$ whereas $T_{1,b} / T_{1a} \simeq 20$. Hence it is the relaxivity (shell thickness multiplied by its relaxation rate $\rho=x/T_{1s}$) which is different between the two kind of droplets $\rho_b / \rho_a \simeq 0.065$. This could indicate that one has less "iceberg" layers of water molecules in the surface of the bigger droplets and faster dynamics inside the droplet than in the case of smaller droplets. Briefly water molecules loses entropy around a hydrophobic solute by surrounding it in an organized way [12] .

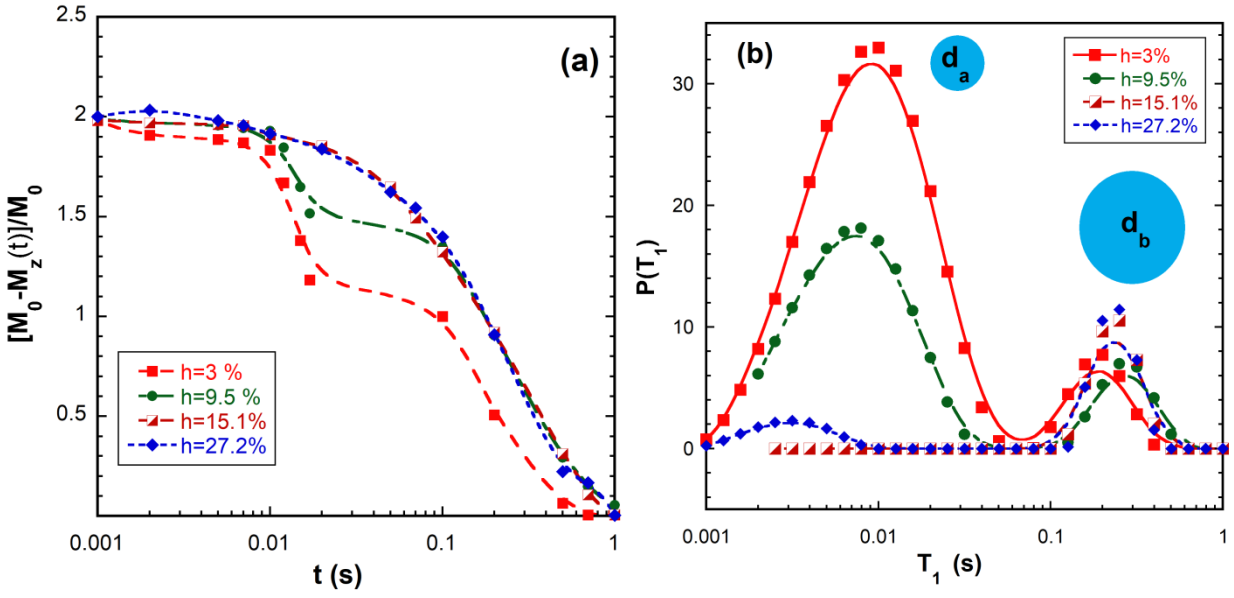

FIGURE 5. (**a**) The decrease of the relative longitudinal nuclear magnetization of heavy water droplets in butyl rubber during an inverse recovery sequence (**b**) Deduced distribution of spin-lattice relaxation T_1 by inverse Laplace transformation from figure 5a.

Figure 6a depicts the variation with temperature of the relative longitudinal deuterium magnetization decrease after an inversion recovery sequence for the sample with hydration h=9.5%. Obviously the dynamics is heterogeneous at high temperature and becomes gradually more homogeneous when cooling down. The numerical Laplace transformation of such decrease is given by figure 6b where one could follow when decreasing temperature, the change of the spin-lattice relaxation time distribution. Clearly one notice that the population with $T_{1,b}$ =200 ms vanish with decreasing temperature which is associated to the crystallization of the droplets with radius r_b~2.2 nm.

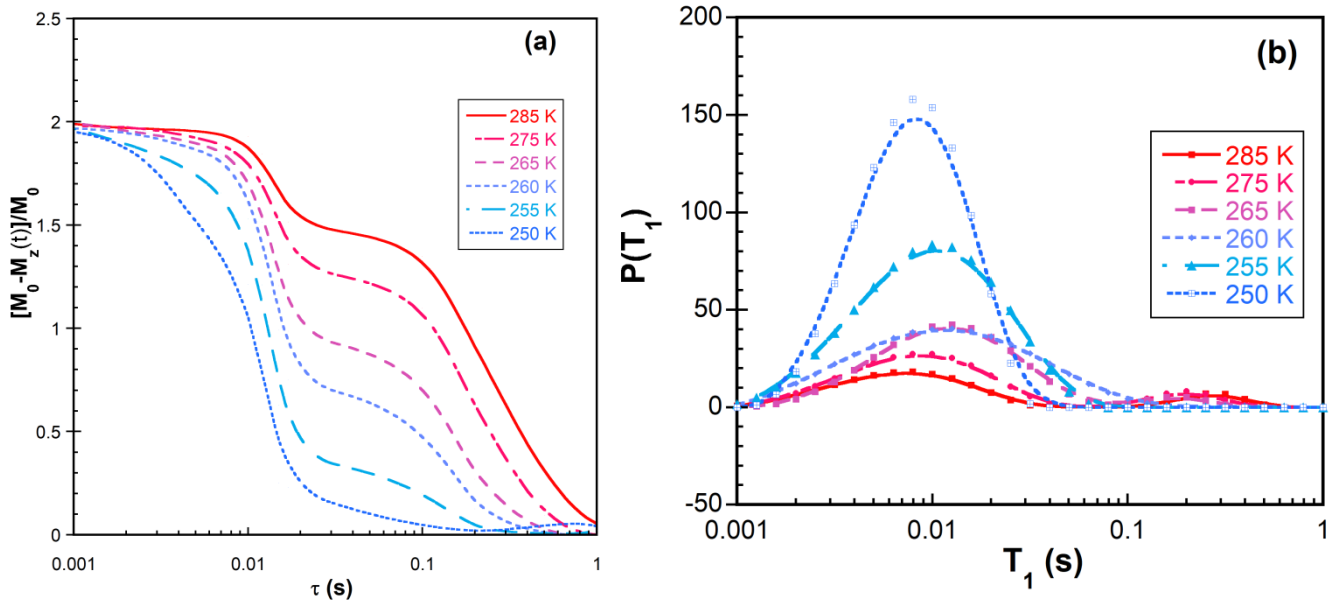

FIGURE 6. (**a**) variation of the relative longitudinal magnetization after an inverse recovery sequence at different temperature for the sample with h=9.5% (**b**) Deduced distribution of spin-lattice relaxation T_1 by inverse Laplace transformation from figure 6a.

From DSC we knew already that hydration ratio changes the population of the two main sizes of droplets. Therefore, one could understand the change of the average overall spin-lattice relaxation depicted in figure 7a as following. When the rubber hydration is progressively increased the relative contribution of the two droplets populations (a) and (b) having respectively the spin-lattice relaxation times $T_{1,a}$ ~10 ms and $T_{1,b}$ ~200 ms at room temperature lies behind this variation of the spin-lattice

relaxation time with hydration rate. First the small droplets are formed and contribute alone to the overall relaxation. At higher hydration one starts to have the formation of droplets with bigger sizes and higher relaxation times which explain the increase of the spin-lattice relaxation time with hydration. Above h~15% the proportion of the two droplet's populations stabilizes and hence the relaxation time remain constant.

The spin-lattice relaxation rate is proportional to the correlation time of the molecular reorientation when fast narrowing condition is satisfied ($\omega_0\tau << 1$) [56]. In such conditions one could write : $R_1 = 1/T_1 \simeq \left(3\omega_Q^2/16\right)\cdot\tau$ where $\omega_Q = e^2qQ/(2I-1)$ is the quadrupole coupling constant. For heavy water the quadrupole coupling constant of deuterium with the local electric field of the polarized O-D bond is about $\nu_Q \simeq 200$ kHz , so the overall relaxation rate could be converted into correlation times as depicted in figure 7b. Although the glass transition of butyl rubber remains constant when changing hydration, the curvature of the plot in Figure 7b suggest that the fragile - strong transition temperature changes as we change the relative populations of droplets. In fact, it was already proven that this temperature where the dynamical behavior of water changes from VFT to Arrhenius, decreases when increasing pressure [41]. Therefore, when the mean size of droplets decreases (by decreasing hydration) the Laplace pressure ($\Delta p = 2\gamma_{lg}/r$ with $\gamma_{lg} \simeq 69.2\ mN/m$ [38]) is higher and the fragile-strong transition temperature is lower which could explain the change with hydration of curves in figure 6b. The fragile – strong transition temperature T_s is well approximated by the intersection of the two behavior. Hence it could be deduced from the equality between the Arrhenius ($\tau_s = \tau_0 \cdot e^{E_a/(RT)}$) and Vogel-Fulcher-Tammann (VFT) $\tau_f = \tau_0 \cdot e^{D.T_0/(T-T_0)}$ equations. In both relations The prefactor τ_0 = 0,01 ps is the typical phonon time

scale . In both type of behavior (strong or fragile, the glass transition temperature T_g corresponds to a slowdown of the molecular motion $\tau(T_g) = 10^2 \cdot s$.

$$\frac{1}{T_s} = \frac{1}{T_0} - \frac{R}{E_a} \cdot D \qquad (5)$$

This transition associated with a crossover of the fragility of the system (from fragile to strong) is found essentially in confined systems and hence some authors considered that it is a finite size effect [62]. One could in all cases estimate the change of fragility coefficient as following : supposing that T_0 which is also the "thermodynamic" Kauzmann temperature T_k remains constant, and since the glass transition temperature is related to the fragility by [63] : $(T_g - T_0)/T_0 = D_f/(17\ln 10)$ then by differentiation we could deduce the change in fragility during this crossover $(T_s - T_g)/T_0 = (D_s - D_f)/(17\ln 10)$. In our case the variation of T_s when reducing the mean droplet size is associated with different changes of fragility during this crossover due of course to different degree of confinement.

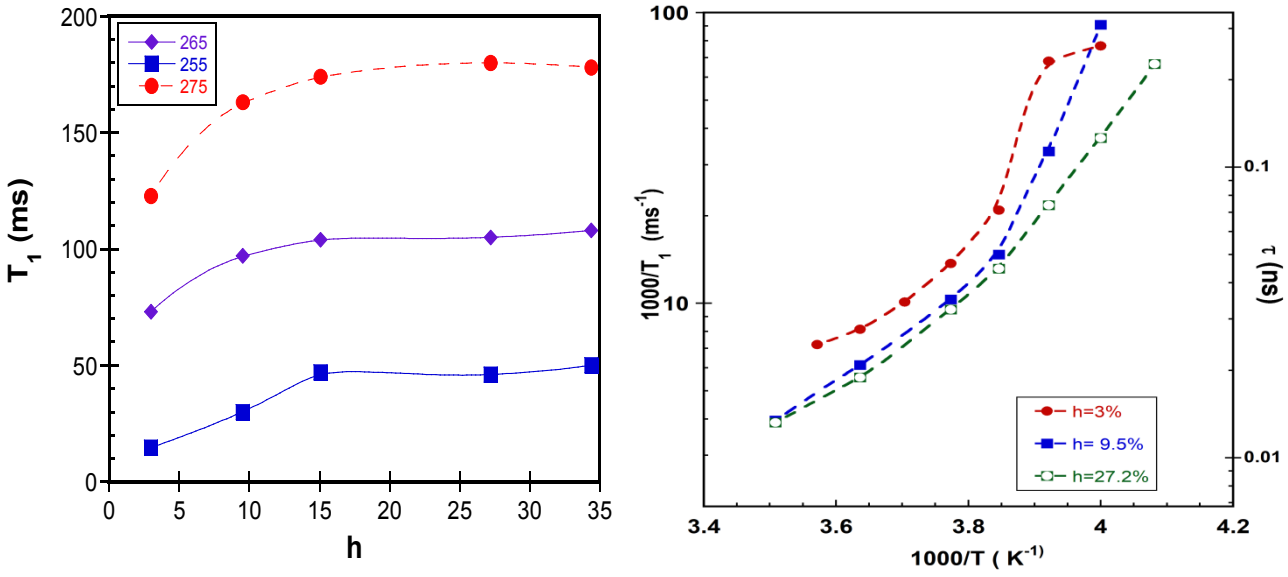

FIGURE 7. (**a**) The variation of the spin-lattice relaxation time with hydration. (**b**) The correlation time of water molecules reorientation and the spin-lattice relaxation rate versus 1000/T for different hydration rate of butyl rubber

CONCLUSION

Water forms nano-droplets around hydrophilic centers when forced to inter hydrophobic elastomers. This system offers the possibility of studying the freezing and melting of these nano droplets as well as the dynamic of supper cooled water confined in hydrophobic surrounding (butyl rubber elastomers). The glass transition of the rubbery matrix remains constant when changing the hydration ratio supporting the fact that water is not dispersed but concentrated around hydrophilic sites as droplets. Another experimental confirmation is also obtained from annealing in the crystallization interval where one showed that we could fractionate the crystallization peak and hence the temperature scale could be converted into droplets size scale. The droplet size distribution of water in butyl rubber is found to be bimodal around two typical sizes d_a=3.4 nm and d_b=4.4 nm in agreement with previous X rays measurements. Despite these small crystal sizes melting is not shifted according to Gibbs-Thomson equation. This fact is explained by an additional positive chemical potential $\Delta\mu$ due to the hydrophobic surrounding. Due to this droplet size distribution, the reorientation dynamics of heavy water is heterogeneous, hence measuring ^2H spin-lattice relaxation rates at different temperatures and hydrations it was possible to probe the dynamics of the super cooled water confined in this hydrophobic matrix.

One finds also a bimodal distribution of relaxation times typically at room temperature $T_{1,a}$ ~10 ms and $T_{1,b}$ ~200 ms. These relaxation time distributions change when lowering temperature due to partial crystallization of the bigger droplets. Finley the dynamics of water in the temperature range 285 k down to 245 k is found to be according VFT but with different T_g and fragility as we decrease the mean droplet size by decreasing the elastomer hydration. All water crystalizes below 235 k prohibiting us to probe its dynamics in the no man land regions as it is the case of hydrophilic confining matrix where a fraction of water never crystalizes even below 235 K.

ACKNOWLEDGMENTS

Dr. R. Neffati extends his appreciation to the Deanship of Scientific Research at King Khalid University for financial support through research groups program under grant number (R.G. P2/81/41). The authors thanks Prof. L. Apekis and Prof. R. Pelster for their assistance and help.

REFERENCES

[1] P. Ball, J Chemical reviews 108 (2008) 74.
[2] M.-C. Bellissent-Funel, Comptes Rendus Geoscience 337 (2005) 173.
[3] M. Shaat, Y. Zheng, Sci Rep 9 (2019) 5689.
[4] D. Chandler, Nature (London) 437 (2005) 640.
[5] E.E. Meyer, K.J. Rosenberg, J. Israelachvili, Proceedings of the National Academy of Sciences of the United States of America 103 (2006) 15739.
[6] M.C. Bellissent-Funel, A. Hassanali, M. Havenith, R. Henchman, P. Pohl, F. Sterpone, D. van der Spoel, Y. Xu, A.E. Garcia, Chem. Rev. 116 (2016) 7673.
[7] R. Zana, Dynamics of Surfactant Self-Assemblies : Micelles, Microemulsions, Vesicles and Lyotropic Phases. Taylor and Francis, 2005.
[8] A. Thomas, K. Muniandy, Poly 28 (1987) 408.
[9] R. Neffati, L. Apekis, J. Rault, Journal of thermal analysis calorimetry 54 (1998) 741.
[10] W. Kauzmann, Advances in protein chemistry, Elsevier, 1959, p. 1-63.
[11] C. Tanford, The hydrophobic effect : Formation of micelles and biological membranes. Wiley, 1980.
[12] F. Franks, Aqueous Solutions of Amphiphiles and Macromolecules. Springer US 1975.
[13] W. Blokzijl, J.B. Engberts, Angewandte Chemie International Edition in English 32 (1993) 1545.
[14] N.T. Southall, K.A. Dill, A. Haymet, ACS Publications, 2002.
[15] G. Némethy, H.A. Scheraga, The Journal of Chemical Physics 36 (1962) 3401.
[16] L.R. Pratt, Annu. Rev. Phys. Chem. 53 (2002) 409.
[17] D. Chandler, Natur 437 (2005) 640.
[18] K. Lum, D. Chandler, J.D. Weeks, J. Phys. Chem. B 103 (1999) 4570.
[19] D. Borgis, S. Luukkonen, L. Belloni, G. Jeanmairet, J. Phys. Chem. B 124 (2020) 6885.
[20] J. Deschamps, F. Audonnet, N. Brodie-Linder, M. Schoeffel, C. Alba-Simionesco, PCCP 12 (2010) 1440.
[21] K. Morishige, The Journal of Physical Chemistry C 122 (2018) 5013.
[22] J. Jelassi, H.L. Castricum, M.C. Bellissent-Funel, J. Dore, J.B. Webber, R. Sridi-Dorbez, Phys. Chem. Chem. Phys. 12 (2010) 2838.
[23] C.G. Wiener, Z. Qiang, Y. Xia, M. Tyagi, B.D. Vogt, PCCP 20 (2018) 28019.
[24] X. Zhang, Y. Zhu, S. Granick, Sci. Cult. 295 (2002) 663.
[25] V. Bianco, G. Franzese, Sci Rep 4 (2014) 4440.
[26] E.G. Strekalova, M.G. Mazza, H.E. Stanley, G. Franzese, J Phys Condens Matter 24 (2012) 064111.
[27] S. Sharma, P.G. Debenedetti, Proc Natl Acad Sci U S A 109 (2012) 4365.
[28] E.B. Moore, J.T. Allen, V. Molinero, The Journal of Physical Chemistry C 116 (2012) 7507.
[29] K. Koga, H. Tanaka, J. Chem. Phys. 122 (2005) 104711.
[30] O. Beckstein, M.S. Sansom, Proceedings of the National Academy of Sciences of the United States of America 100 (2003) 7063.

[31] J.M. Zanotti, P. Judeinstein, S. Dalla-Bernardina, G. Creff, J.B. Brubach, P. Roy, M. Bonetti, J. Ollivier, D. Sakellariou, M.C. Bellissent-Funel, Sci Rep 6 (2016) 25938.
[32] G. Briggs, D. Edwards, E. Storey, Rubber Chemistry Technology 36 (1963) 621.
[33] R. Pelster, A. Kops, G. Nimtz, A. Enders, H. Kietzmann, P. Pissis, A. Kyritsis, D. Woermann, Berichte der Bunsengesellschaft für physikalische Chemie 97 (1993) 666.
[34] A.Y. Coran, Science and technology of rubber, Elsevier, 1994, p. 339-385.
[35] K. Sangwal, Nucleation and crystal growth : metastability of solutions and melts. John Wiley & Sons, 2018.
[36] J. Rault, A. Lucas, R. Neffati, M. Monleón Pradas, Macromolecules 30 (1997) 7866.
[37] S. Mascotto, W. Janke, R. Valiullin, The Journal of Physical Chemistry C 121 (2017) 23788.
[38] T. Li, D. Donadio, G. Galli, Nat Commun 4 (2013) 1887.
[39] J. Swenson, PCCP 20 (2018) 30095.
[40] R. Shi, J. Russo, H. Tanaka, Proc Natl Acad Sci U S A 115 (2018) 9444.
[41] L. Liu, S.-H. Chen, A. Faraone, C.-W. Yen, C.-Y. Mou, Phys. Rev. Lett. 95 (2005) 117802.
[42] F. Mallamace, M. Broccio, C. Corsaro, A. Faraone, U. Wanderlingh, L. Liu, C.Y. Mou, S.H. Chen, J. Chem. Phys. 124 (2006) 161102.
[43] F. Mallamace, M. Broccio, C. Corsaro, A. Faraone, L. Liu, C.-Y. Mou, S.-H. Chen, J. Phys.: Condens. Matter 18 (2006) S2285.
[44] M. Vogel, The European Physical Journal Special Topics 189 (2010) 47.
[45] J. Korb, NJPh 13 (2011) 035016.
[46] R. Kimmich, NMR: tomography, diffusometry, relaxometry. Springer Science & Business Media, 2012.
[47] A. Valori, B. Nicot, J Petrophysics 60 (2019) 255.
[48] O.V. Petrov, I. Furó, J Microporous mesoporous materials 136 (2010) 83.
[49] R. Neffati, P. Judeinstein, J. Rault, J Phys Condens Matter 32 (2020) 465101.
[50] M. Botev, P. Judeinstein, R. Neffati, J. Rault, Macromolecules 29 (1996) 8538.
[51] M. Botev, R. Neffati, J. Rault, Polymer 40 (1999) 5227.
[52] K.R. Brownstein, C. Tarr, J Physical review A 19 (1979) 2446.
[53] A.Y. Coran, Rubber chemistry technology 68 (1995) 351.
[54] M.a. Akiba, A.J.P.i.p.s. Hashim, 22 (1997) 475.
[55] M. Brun, A. Lallemand, J.-F. Quinson, C. Eyraud, Thermochim. Acta 21 (1977) 59.
[56] R.K. Harris, Nuclear Magnetic Resonance Spectroscopy. Longman Pub Group, England, 1986.
[57] J. Mitchell, J. Webber, J. Strange, PhR 461 (2008) 1.
[58] J. Rault, R. Neffati, P. Judeinstein, The European Physical Journal B-Condensed Matter and Complex Systems 36 (2003) 627.
[59] R. Defay, I. Prigogine , A. Bellemans, Surface Tension and Adsorption. longmans, 1966.
[60] S.W. Provencher, Comput. Phys. Commun. 27 (1982) 213.
[61] F. Franks, Water and Aqueous Solutions at Subzero Temperatures. Springer US, 1982.
[62] S. Cerveny, J. Colmenero, A. Alegria, Phys. Rev. Lett. 97 (2006) 189802; discussion 189803.
[63] C. Angell, Chem. Rev. 102 (2002) 2627.

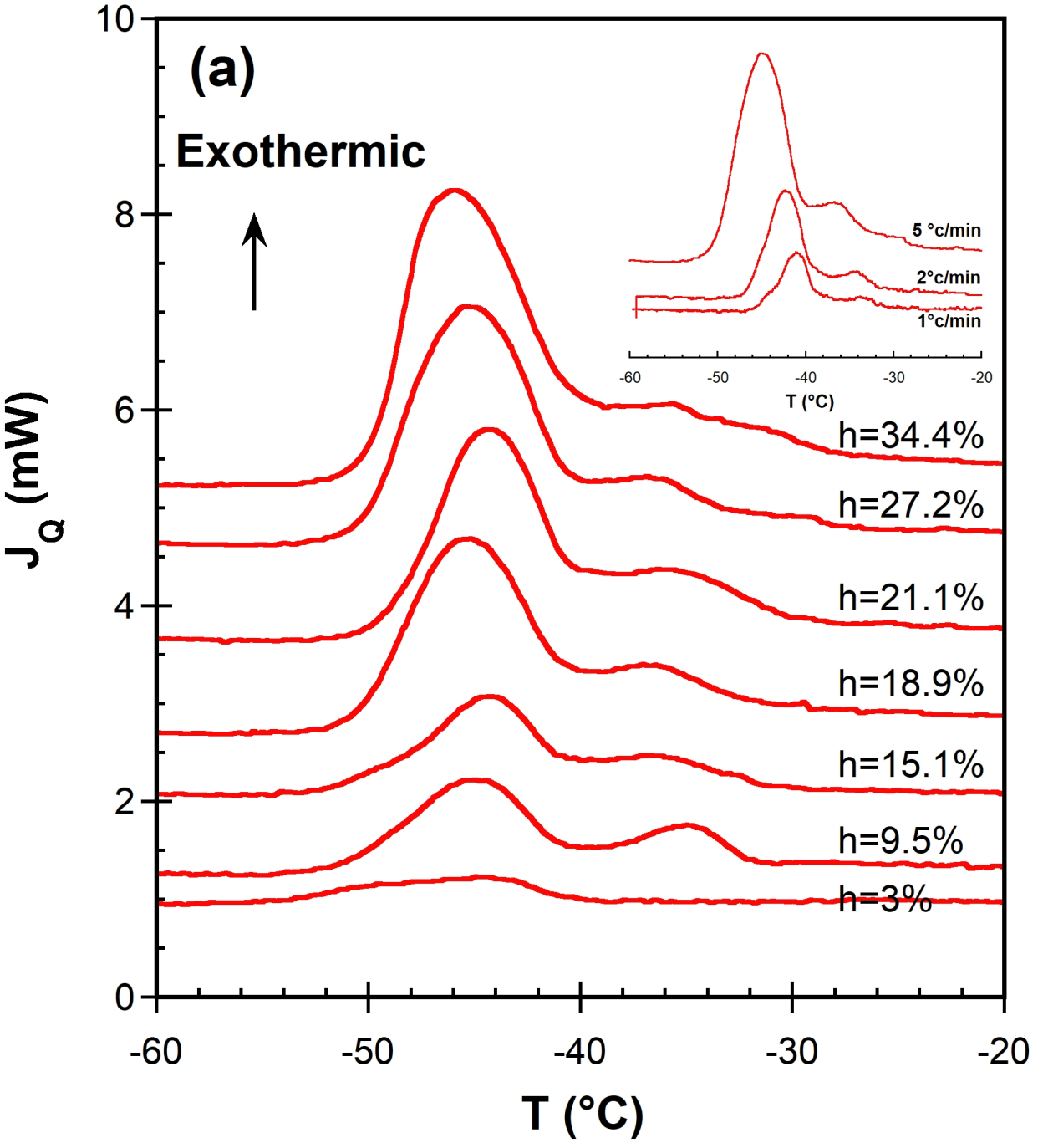
(a)
Exothermic
5 °c/min
2°c/min
1°c/min
T (°C)
h=34.4%
h=27.2%
h=21.1%
h=18.9%
h=15.1%
h=9.5%
h=3%
J_Q (mW)
T (°C)

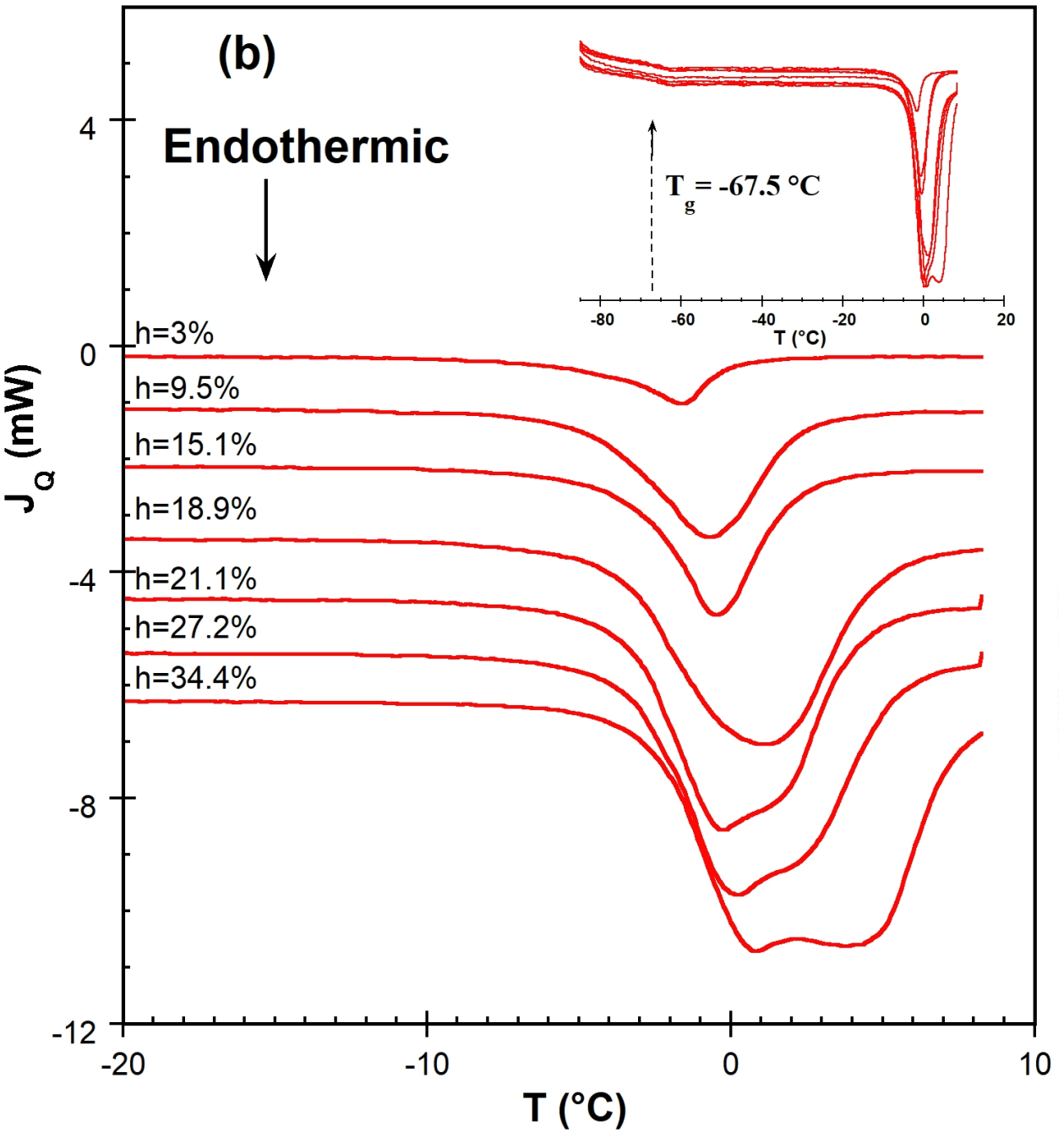
(b)
Endothermic
T_g = -67.5 °C
T (°C)
h=3%
h=9.5%
h=15.1%
h=18.9%
h=21.1%
h=27.2%
h=34.4%
J_Q (mW)
T (°C)

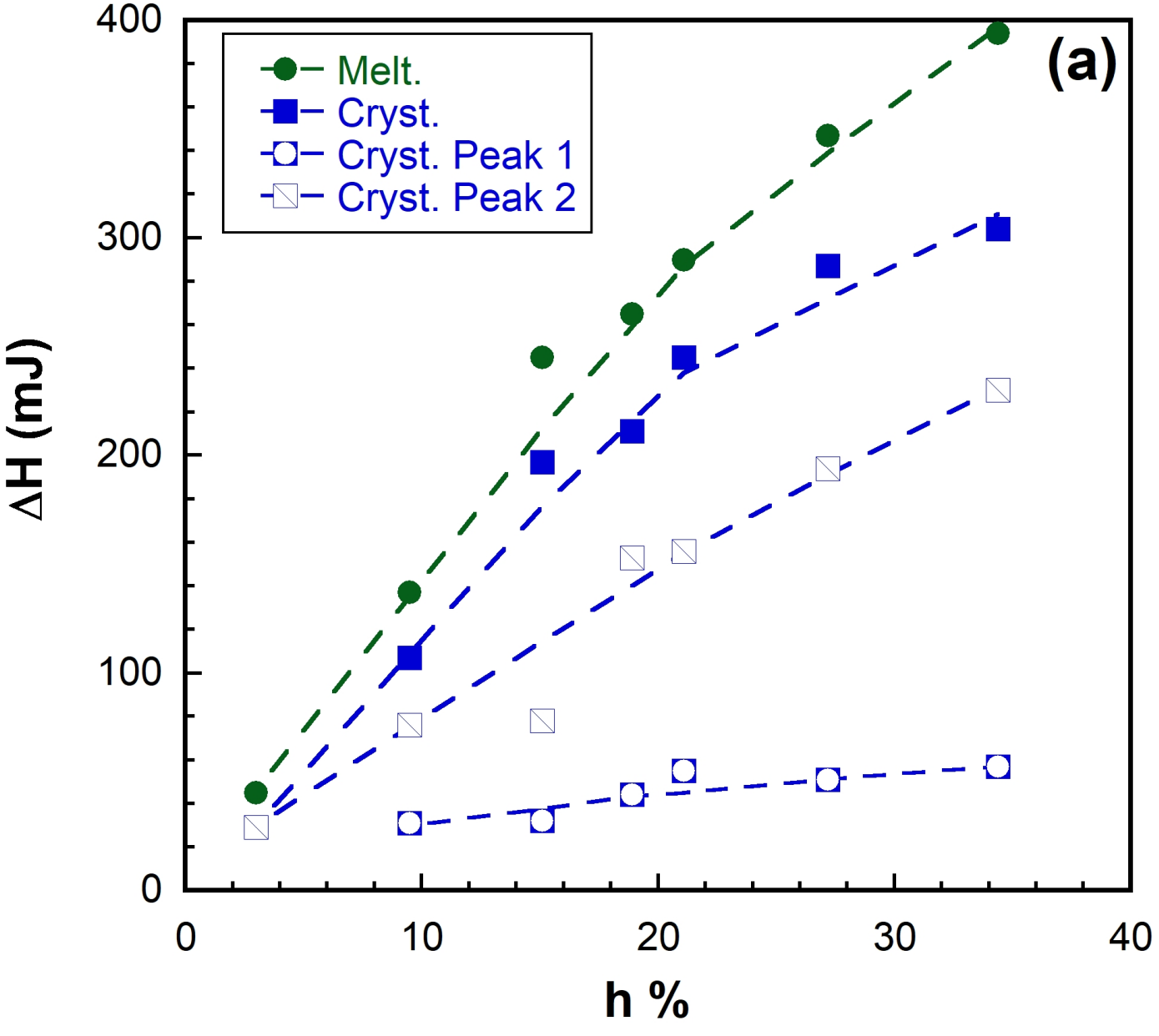
Melt.
Cryst.
Cryst. Peak 1
Cryst. Peak 2
(a)
ΔH (mJ)
h %
0
100
200
300
400
0
10
20
30
40

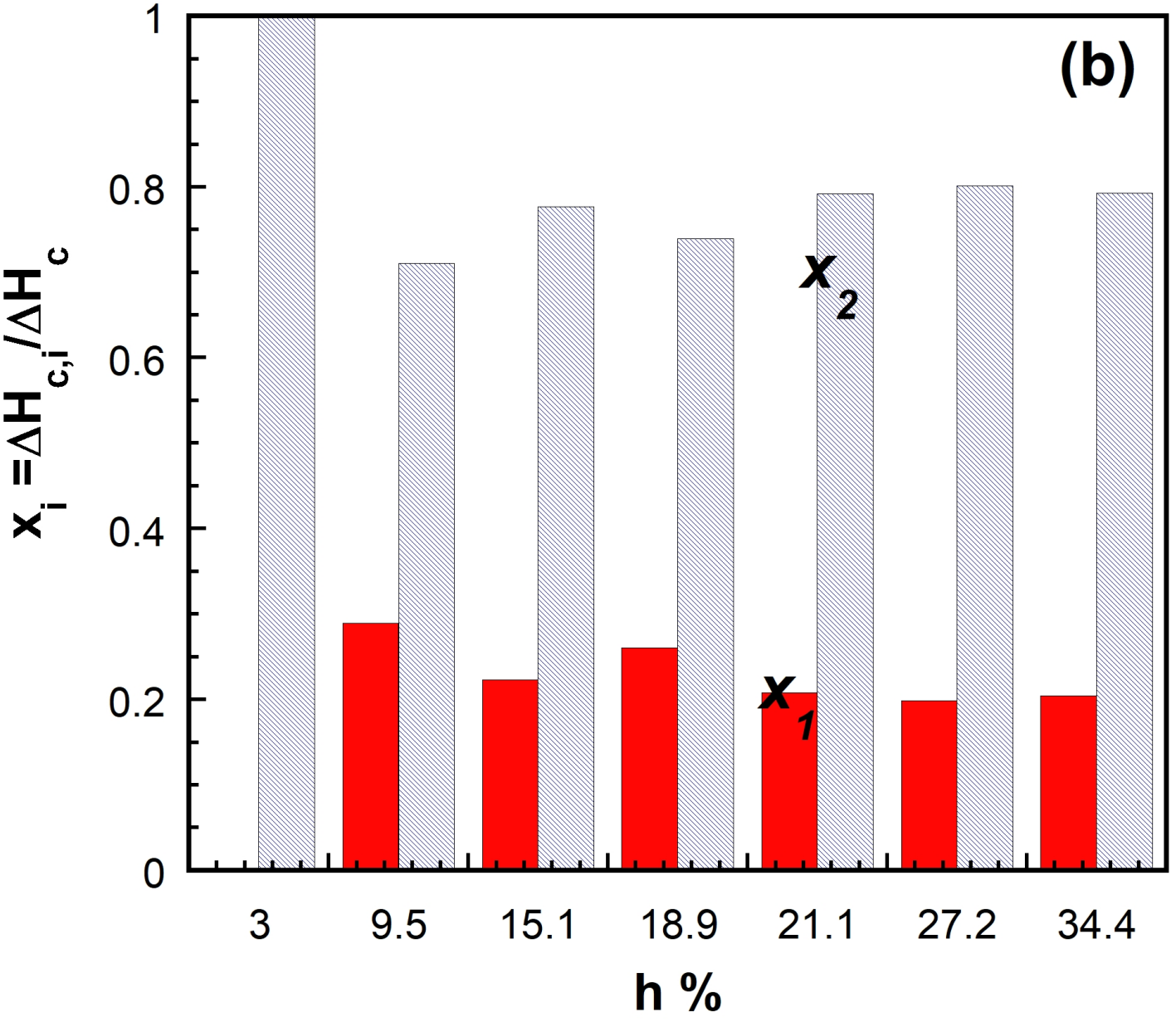
(b)
$x_i = \Delta H_{c,i} / \Delta H_c$
1
0.8
0.6
0.4
0.2
0
x_2
x_1
3
9.5
15.1
18.9
21.1
27.2
34.4
h %

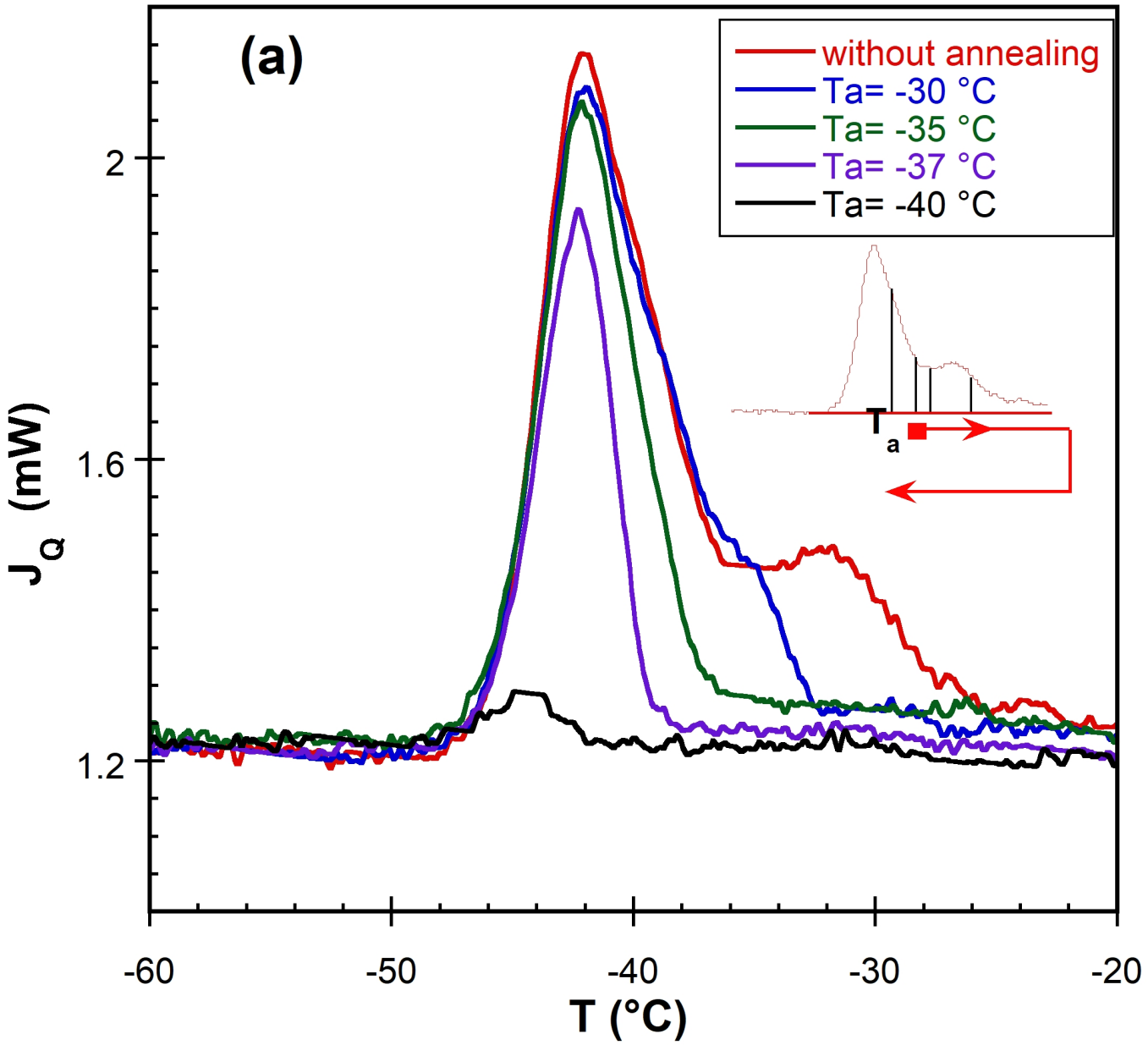
(a)
without annealing
Ta= -30 °C
Ta= -35 °C
Ta= -37 °C
Ta= -40 °C
T
a
2
1.6
1.2
J_Q (mW)
-60
-50
-40
-30
-20
T (°C)

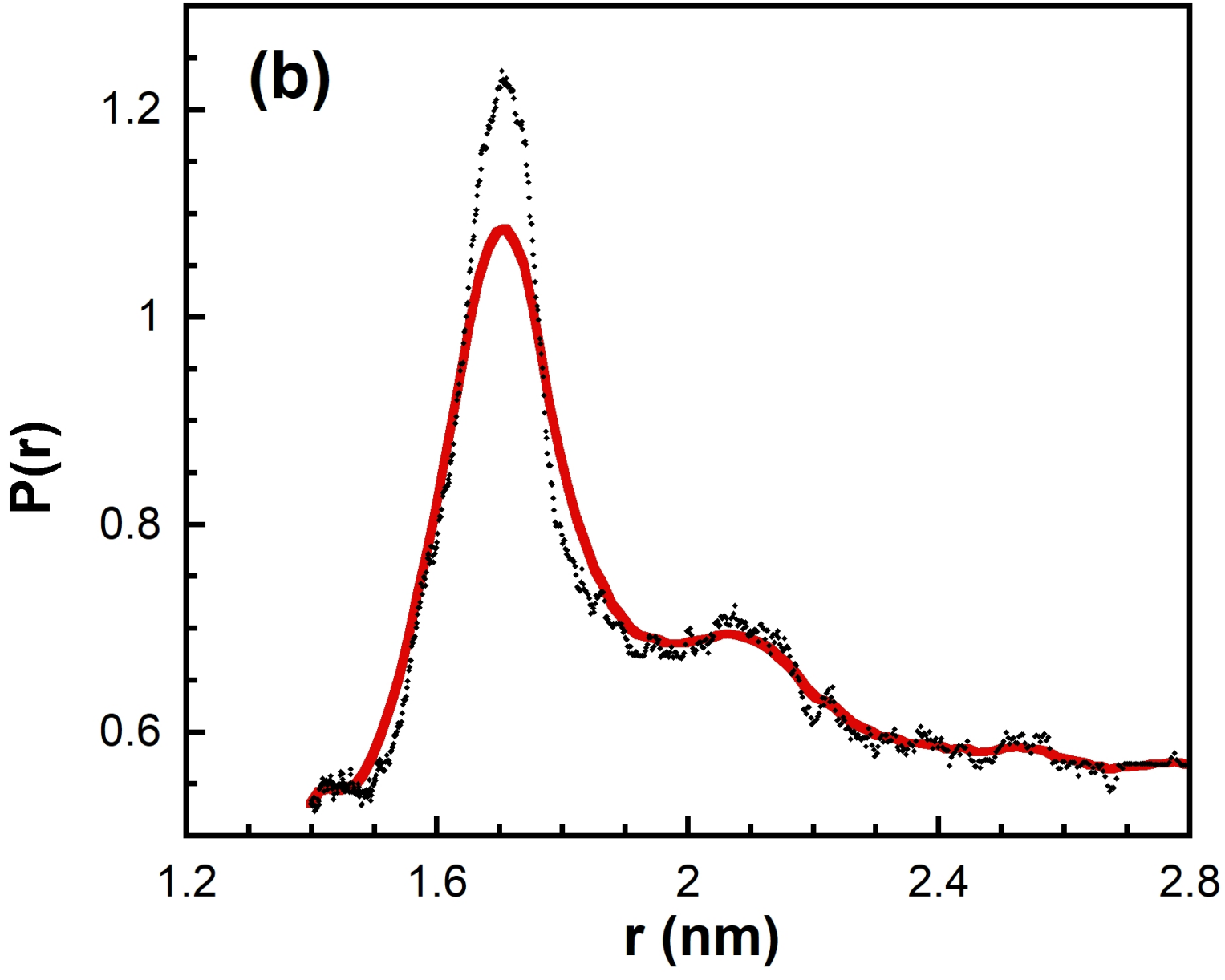
(b)
1.2
1
0.8
0.6
P(r)
1.2
1.6
2
2.4
2.8
r (nm)

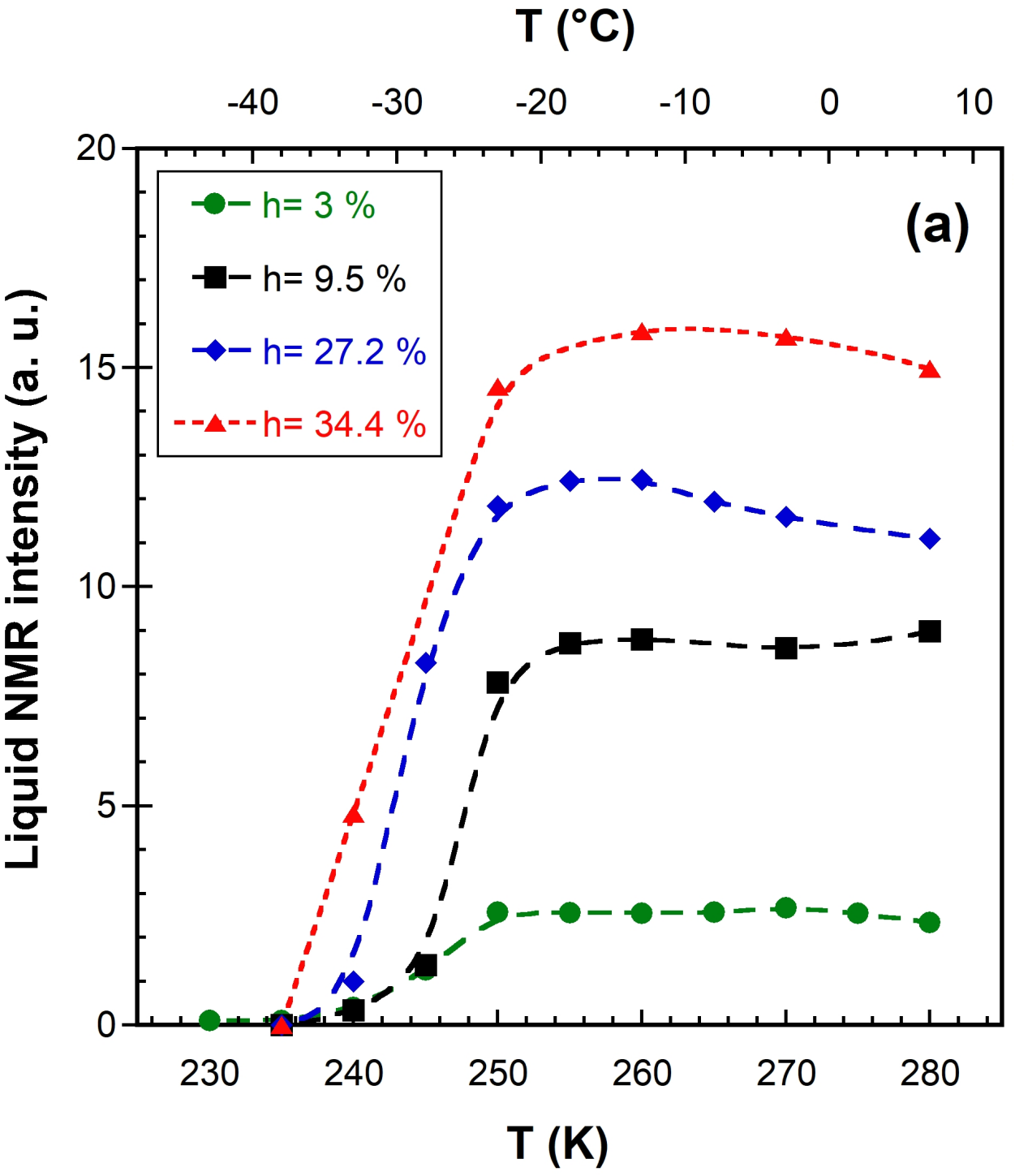
T (°C)
-40
-30
-20
-10
0
10
20
15
10
5
0
Liquid NMR intensity (a. u.)
h= 3 %
h= 9.5 %
h= 27.2 %
h= 34.4 %
(a)
230
240
250
260
270
280
T (K)

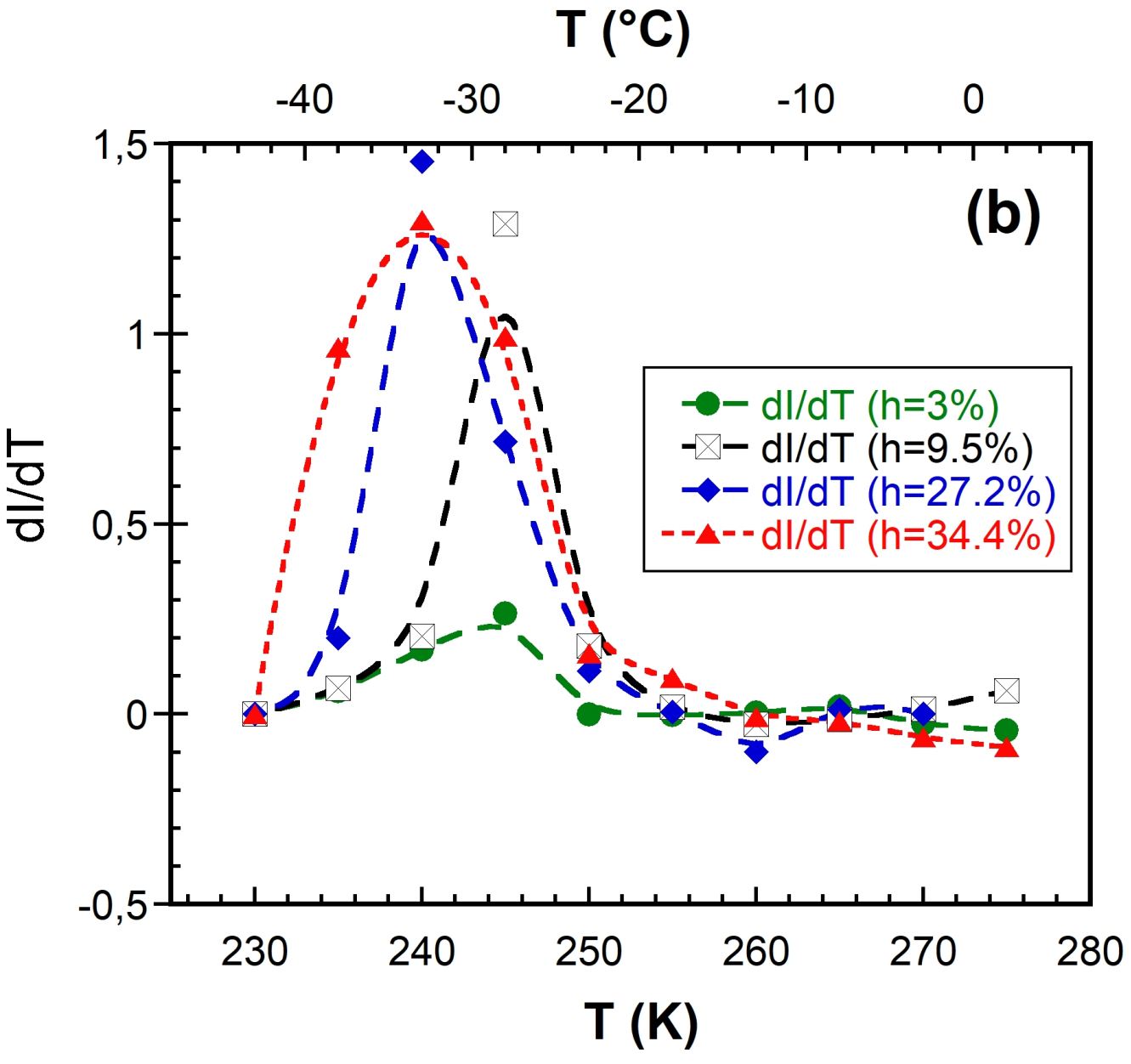
T (°C)
-40
-30
-20
-10
0
(b)
dI/dT
1,5
1
0,5
0
-0,5
dI/dT (h=3%)
dI/dT (h=9.5%)
dI/dT (h=27.2%)
dI/dT (h=34.4%)
230
240
250
260
270
280
T (K)

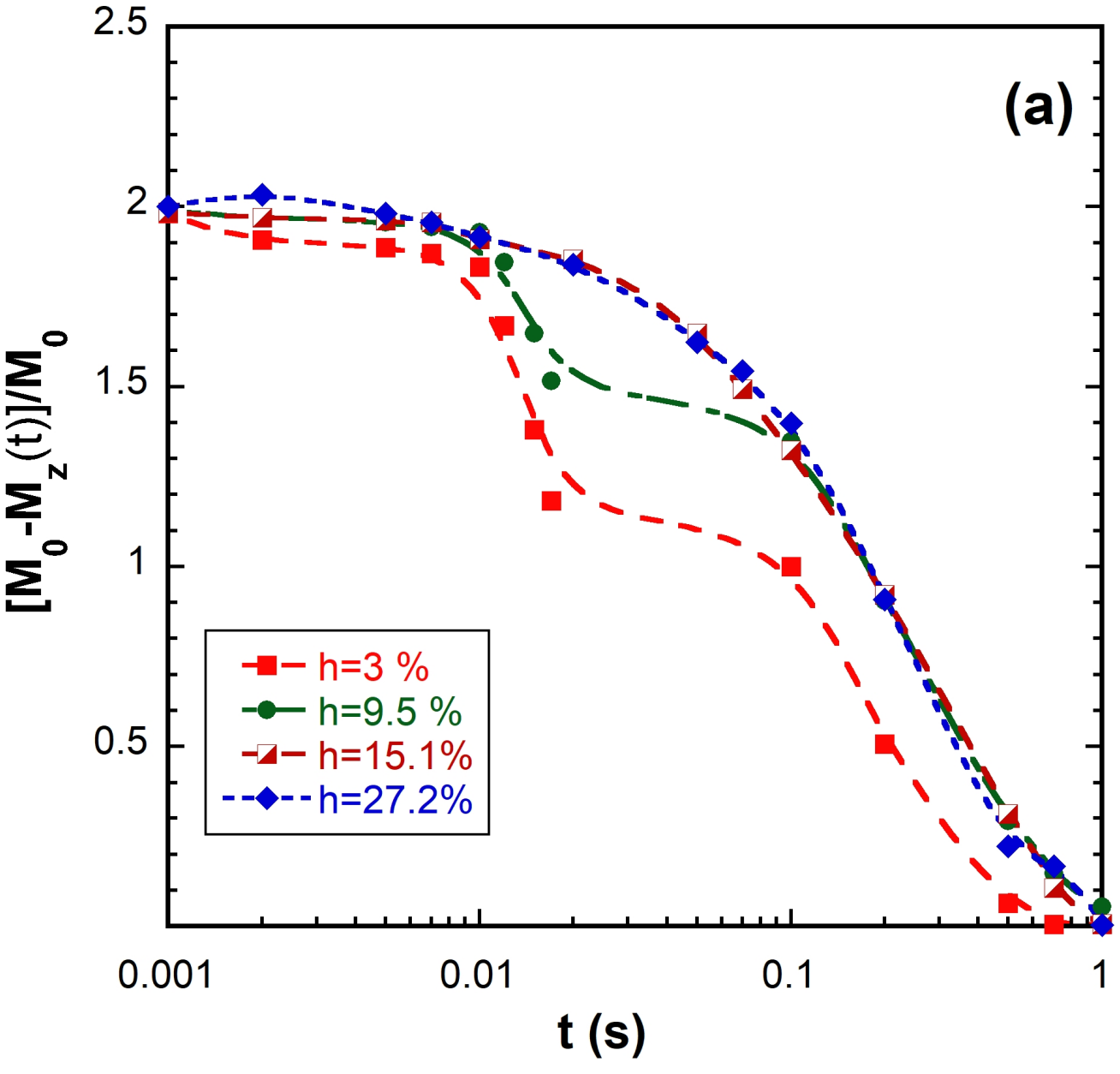
(a)
2.5
2
1.5
1
0.5
0.001
0.01
0.1
1
t (s)
[M0-Mz(t)]/M0
h=3 %
h=9.5 %
h=15.1%
h=27.2%

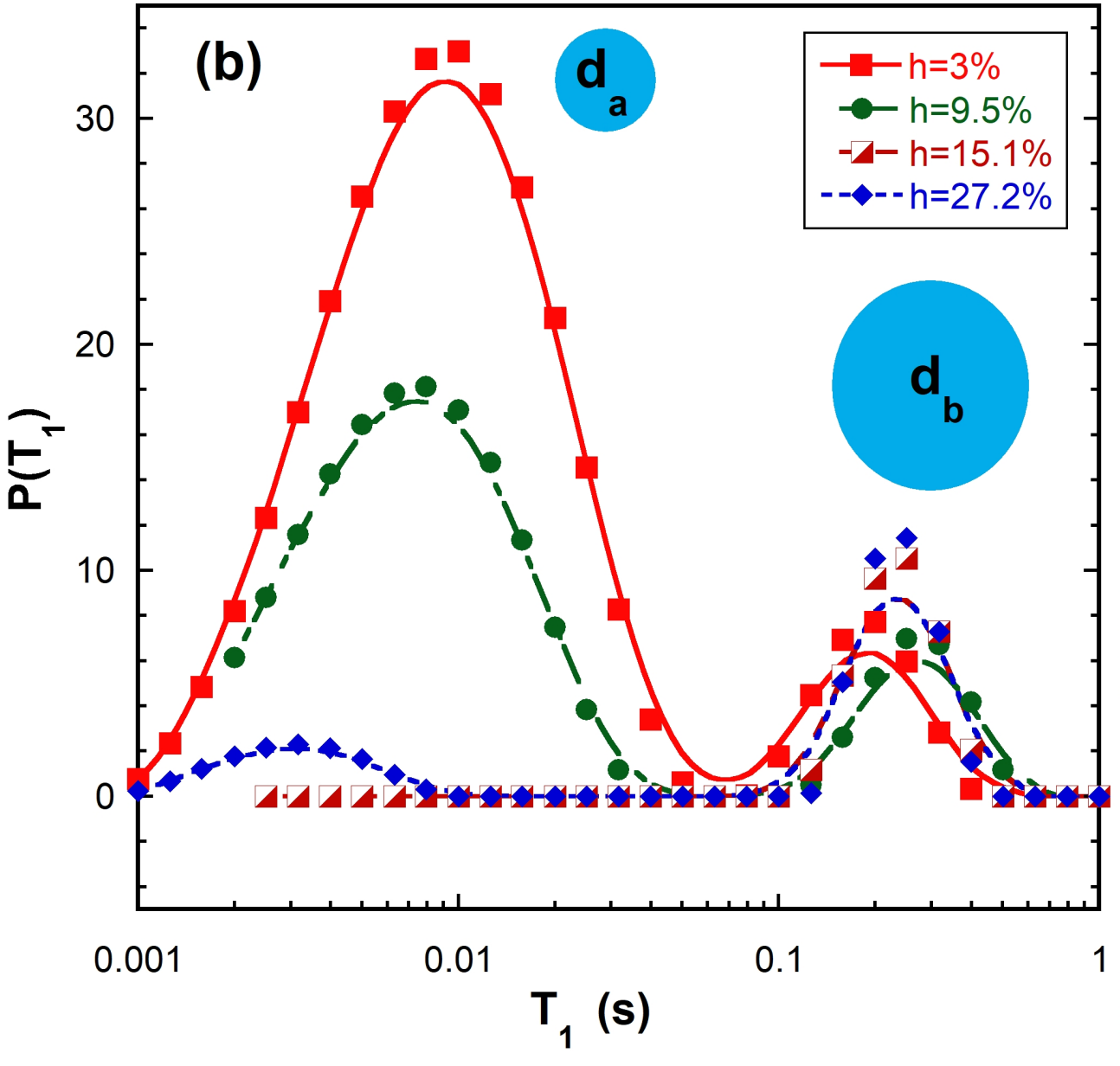
(b)
d a
d b
h=3%
h=9.5%
h=15.1%
h=27.2%
P(T1)
30
20
10
0
0.001
0.01
0.1
1
T1 (s)

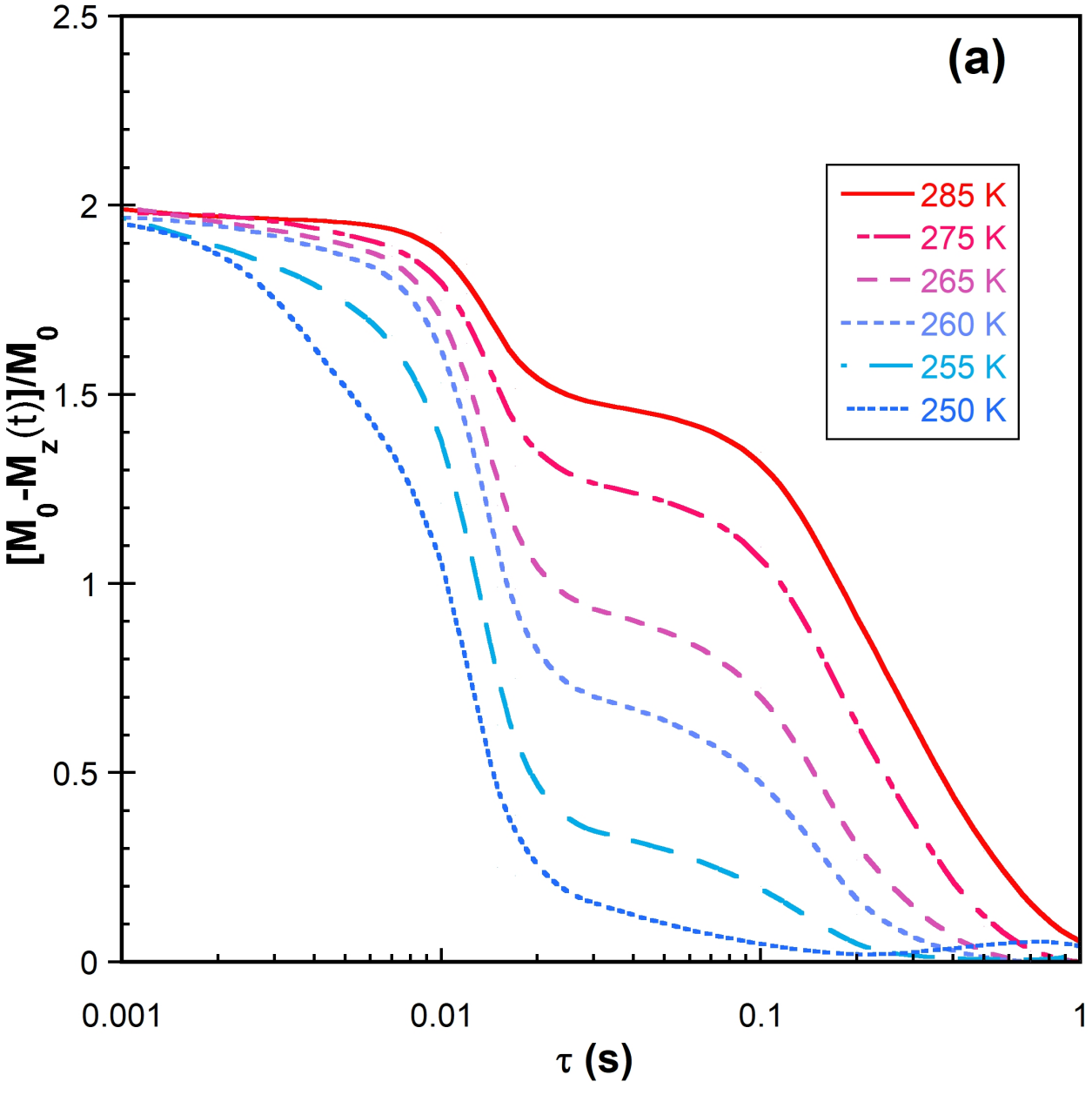
(a)
285 K
275 K
265 K
260 K
255 K
250 K
[M0-Mz(t)]/M0
τ (s)
2.5
2
1.5
1
0.5
0
0.001
0.01
0.1
1

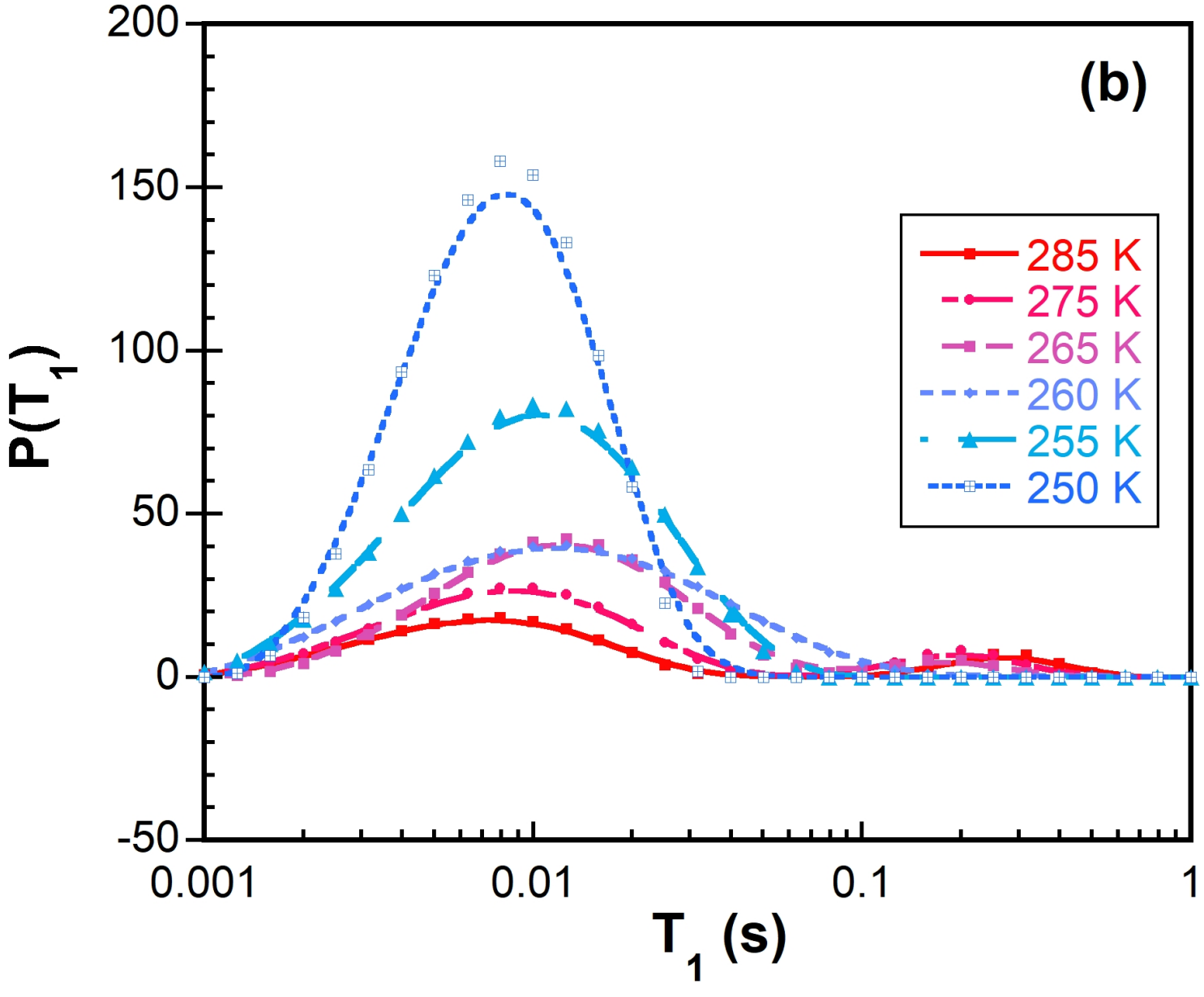
(b)
285 K
275 K
265 K
260 K
255 K
250 K
P(T1)
T1 (s)
200
150
100
50
0
-50
0.001
0.01
0.1
1

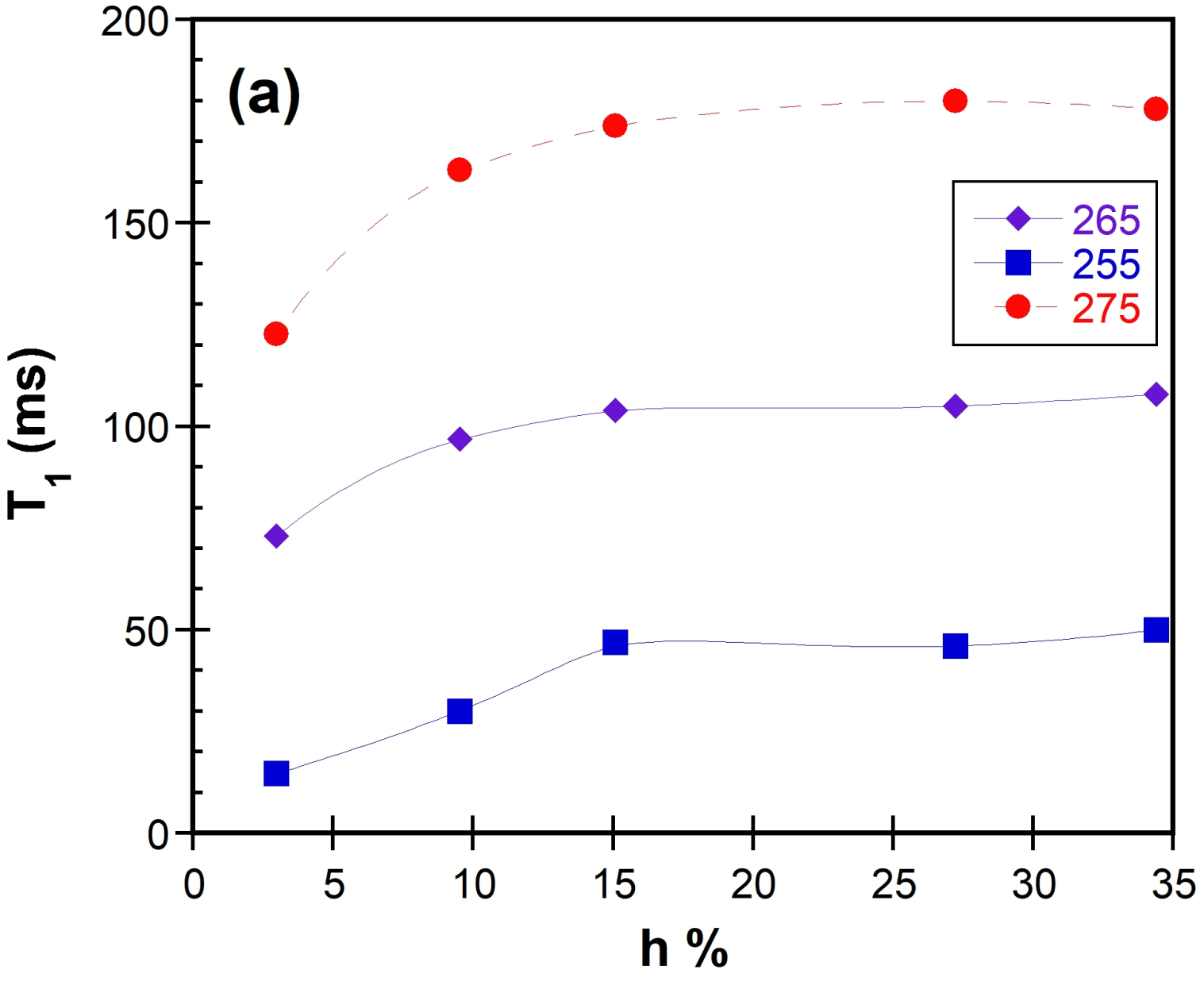
(a)
200
150
100
50
0
T_1 (ms)
0
5
10
15
20
25
30
35
h %
265
255
275

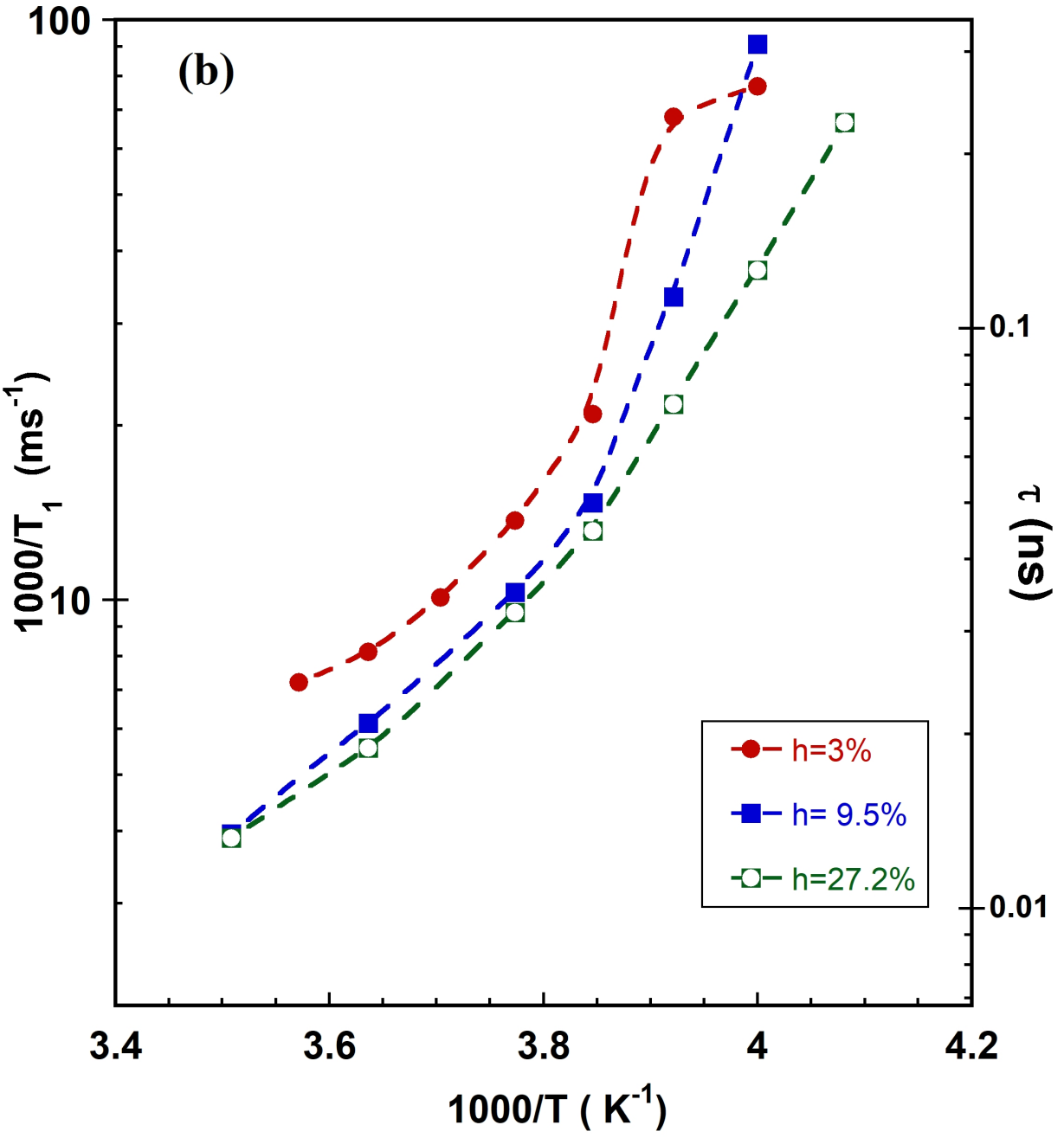
(b)
100
10
0.1
0.01
1000/T$_1$ (ms^{-1})
(su) $_1$
3.4
3.6
3.8
4
4.2
1000/T (K^{-1})
h=3%
h= 9.5%
h=27.2%

Declaration of interests

 The authors declare that they have no known competing financial interests or personal relationships that could have appeared to influence the work reported in this paper.

☐The authors declare the following financial interests/personal relationships which may be considered as potential competing interests: